The Catalytic Performance of Ni-Co/Beta Zeolite Catalysts in Fischer-Tropsch Synthesis

Renata Sadek [1,2], **Karolina A. Chalupka** [1,*], **Pawel Mierczynski** [1], **Waldemar Maniukiewicz** [1], **Jacek Rynkowski** [1], **Jacek Gurgul** [3], **Magdalena Lasoń-Rydel** [4], **Sandra Casale** [2], **Dalil Brouri** [2] and **Stanislaw Dzwigaj** [2,*]

[1] Institute of General and Ecological Chemistry, Lodz University of Technology, Zeromskiego 116, 90-924 Lodz, Poland; renata.sadek90@gmail.com (R.S.); pawel.mierczynski@p.lodz.pl (P.M.); waldemar.maniukiewicz@p.lodz.pl (W.M.); jacek.rynkowski@p.lodz.pl (J.R.)

[2] Laboratoire de Réactivité de Surface, Sorbonne Université-CNRS, UMR 7197, 4 Place Jussieu, Case 178, F-75252 Paris, France; sandra.casale@upmc.fr (S.C.); dalil.brouri@upmc.fr (D.B.)

[3] Jerzy Haber Institute of Catalysis and Surface Chemistry, Polish Academy of Sciences, Niezapominajek 8, PL-30239 Krakow, Poland; ncgurgul@cyf-kr.edu.pl

[4] Łukasiewicz Research Network—Institute of Leather Industry, Products, Processes and Environment Laboratory, Laboratory of Environment, Zgierska 73, 91-462 Łódź, Poland; m.rydel@ips.lodz.pl

* Correspondence: karolina.chalupka@p.lodz.pl (K.A.C.); stanislaw.dzwigaj@upmc.fr (S.D.); Tel.: +48-426-313-125 (K.A.C.); +33-144-272-113 (S.D.)

check for updates

Abstract: The influence of nickel introduction on the catalytic performance of cobalt micro- and mesoporous Beta zeolite catalysts in Fischer–Tropsch Synthesis was studied. Catalysts containing 3 wt% of nickel and 10 wt% of cobalt were prepared by co-impregnation and sequential impregnation and comprehensively characterized by XRD, XPS, NH_3-TPD, TPR-H_2 and TEM EDX techniques. Neither the dealumination of Beta zeolite nor the incorporation of Co and Ni affected its structure, as shown by XRD and BET investigations. The presence of nickel results in the decrease in the temperature of the cobalt oxide reduction, evidenced by TPR-H_2 and the increase of CO conversion. Among all the tested catalysts, the best catalytic properties in FTS showed that based on microporous dealuminated zeolites with a very high CO conversion, near 100%, and selectivity to liquid products of about 75%. In case of dealuminated samples, the presence of Ni decreased the selectivity to liquid products. All catalysts under study showed high resistance to deactivation during the whole time of synthesis (24 h). The very high stability of nickel-cobalt based Beta catalysts was probably due to the hydrogen spillover from metallic nickel particles to cobalt oxides, which decreased re-oxidation of the active phase, sintering and the creation of the carbon on the catalyst surface. Moreover, the presence of Ni on the surface of cobalt-based Beta catalysts could obstruct the formation of graphitic carbon and, in consequence, delay the deactivation of the catalyst.

Keywords: nickel; cobalt; Beta zeolites; Fischer–Tropsch synthesis

1. Introduction

As a result of oil resources reduction, the development and optimization of the alternative fuels production is becoming a very important challenge. One of such processes is the well known Fischer–Tropsch Synthesis (FTS). In this reaction, long-chain hydrocarbons from syngas are formed. The most commonly used catalysts in FTS are iron and cobalt based systems, but the latter exhibits low selectivity to CO_2, enhanced formation of unsaturated hydrocarbons and moderate activity in water–gas shift reaction (WGS) [1–7]. Although oxides such as SiO_2 and Al_2O_3 are usually applied as

a support in this process, zeolites are a very interesting choice due to the presence of acidic sites and high surface area [6–9].

The application of proper support can be the key factor in the activity of discussed catalysts in the described process. It is known that the high activity and selectivity of cobalt catalytic system used in FTS depends on active centers present on the surface of the reduced catalyst. It is conditioned by two main parameters: metal dispersion and the reduction's degree of Co_3O_4 [2,4]. Usually used in FTS, iron- or cobalt-supported catalysts (Fe or Co/SiO_2, Fe or Co/Al_2O_3) lead to the formation of linear hydrocarbons and n-paraffins (waxes), which possess a high cetane number, but a very low octane number. From this reason, the application of zeolite materials as catalysts support in FTS process seems to be justified. These materials possess many specific properties like highly developed specific surface area, the presence of micro- and mesopores, which may improve the metal dispersion inside of micro- and mesoporous channels and allow for obtaining of smaller cobalt crystallites. The well known properties of zeolites in the cracking process may cause the decrease of selectivity towards very long-chain paraffins, which may lead to an increase of the octane number [5,10–13].

Depending on the catalysts used in FTS, a different spectrum of products can be obtained, and this process can be either a low-temperature (Co catalysts) or a high-temperature (Fe catalysts) process. The main advantages of cobalt catalysts are lower carbon deposition and smaller selectivity towards CO_2 than in case of iron catalysts. However, iron catalysts show smaller selectivity towards methane. They also possess an additional self-point which results in lower costs. It should be stressed that both types of FTS catalysts are deactivated by crystallites sintering and carbon deposition formation.

In our previous studies where the Beta zeolite with a high specific surface area was applied as support, the very good dispersion of cobalt and iron metals was observed with the formation of a smaller crystallites size of cobalt (10–16 nm) than iron (ca. 20 nm). This leads to limitation of the sintering process during the activation of the catalyst and carrying out of the reaction. Moreover, the application of the two-step postsynthesis method for the preparation of catalysts allows for a decrease of catalysts acidity and results in the formation of a smaller amount of carbon deposition in comparison to classical oxide-supported catalysts. This promising result encourages the continuation of this investigation and of making attempts to improve the activity and selectivity towards gasoline on CoBeta zeolite catalysts [14,15].

In order to increase the efficiency of FTS catalysts, some promoters are added. It was noticed that the presence of a second metal, e.g., transition or noble metal, could lead to the enhancement of the catalytic activity [1,2]. Many studies have focused a correlation between the active phase of the catalysts and the promoter, and its impact on the course of the Fischer–Tropsch synthesis. The advantages resulting from the promoter addition include the improvement of metal nanoparticles reducibility and dispersion, and consequently, increase the activity and stability of the catalyst in FTS [2,16]. Xiong et al. [17] have reported the effect of zirconium addition (0.5, 1, 5, 9, 15 wt%) to 15 wt% Co/Al_2O_3 catalyst. The authors have claimed that the increase of the Zr loading (>5 wt%) led to the improvement of CO hydrogenation and selectivity to heavy hydrocarbons, which could be linked with the formation of larger cobalt clusters, resulting in more metallic Co active centers. For a low zirconium content (0.5–1.0 wt%), no substantial changes in the creation of C_{5+} hydrocarbons were observed. Moreover, it was shown that increasing the Zr content also led to a rise of the olefin/paraffin ratio as well as a decrease of selectivity towards CH_4.

The positive effect of Zr on the activity of catalyst and selectivity to heavier hydrocarbons was also observed by Ali et al. for $Zr/Co/SiO_2$ [18]. A number of studies have been done to examine the influence of noble metal promoter in cobalt-based catalysts on activity in FTS [19–21]. According to Xu et al. [19], the promotion of 12 wt% Co/Al_2O_3 by metals such as Pt, Pd and Ru leads to the a significant fall in the reduction temperature of oxidic cobalt species. Vada et al. [20] pointed out that the improvement of the reducibility of oxidic Co particles caused by the addition of Re or Pt to 8.7 wt%Co/Al_2O_3 led to an increase in the CO hydrogenation rate. Jacobs et al. [22] investigated the reducibility of 15 wt% Co/Al_2O_3 with the addition of rhenium (0.02–2.5 wt%). Rhenium was found to

promote the second stage of Co_3O_4 reduction, CoO to metallic Co, however, increasing the Re loading above 1 wt% did not cause an additional decrease in the reduction temperature. Xiong et al. [23] have drawn our attention to the impact of ruthenium on activity of Co/SBA-15 with 30 wt% of Co on FTS. The observed phenomenon was related to the fact that the use of an Ru-promoted system resulted in receiving a smaller amount of unreduced cobalt oxides, which are capable of catalyzing the WGS reaction, and hence, an increase of the hydrogen to carbon oxide ratio. According to Wang et al. [2], the addition of Ni or Ru promoter to 20 wt% Co/HZSM-5 catalyst increases both its activity and selectivity towards gasoline-range hydrocarbons. The improvement of the CO conversion is associated with a better dispersion of cobalt and a decrease in the size of cobalt nanoparticles. Ru-promoted 20 wt% Co/HZSM-5 catalyst appeared to be more stable than that promoted with Ni. On the other hand, Rytter et al. [24] observed that nickel addition to alumina-supported Co plays an important role in the stabilization of obtained catalysts.

The study presented in this paper was focused on the analysis of the influence of nickel addition on the activity and selectivity of CoBeta zeolite systems in FTS. This work is a continuation of our previous studies based on cobalt Beta catalysts and focused on the role of the cobalt and type of porosity (micro- and mesoporous) of Beta zeolites on their activity and selectivity in Fischer–Tropsch synthesis [25]. Two types of Beta zeolite, namely micro and mesoporous, were selected as supports for these catalysts. The NiCoBeta and co-NiCoBeta catalysts obtained by sequential and co-impregnation methods, respectively, with different catalytic activities were characterized by X-ray diffraction (XRD), X-ray photoelectron spectroscopy (XPS), temperature- programmed desorption of NH_3 (NH_3-TPD), temperature-programmed reduction of H_2 (TPR-H_2) and Transmission Electron Microscopy with X-Ray Energy Dispersive Spectroscopy (TEM EDX) techniques.

2. Results and Discussion

2.1. Preparation of Different Kind of Catalysts

Different types of Mi-$Ni_{3.0}Co_{10}$AlBeta and Me-$Ni_{3.0}Co_{10}$SiBeta zeolite catalysts were prepared by conventional wet impregnation and the two-step post-synthesis method, respectively (as shown in Scheme 1), where "Mi" stands for microporous, "Me" for mesoporous, "$Ni_{3.0}$" for 3.0 wt% of nickel, "Co_{10}" for 10 wt% of cobalt, "AlBeta" for aluminated Beta zeolite and "SiBeta" for dealuminated Beta zeolite. In order to obtain these zeolite catalysts, Mi- and Me-tetraethylammonium Beta (Mi-TEABeta and Me-TEABeta) zeolites produced by RIPP (China) were divided into two fractions.

The first fraction was calcined in air for 15 h at 550 °C to obtain HAlBeta supports, mesoporous with Si/Al ratio of 18 (Me-HAlBeta) and microporous with Si/Al ratio of 18 (Mi-SiBeta). The Me-$Ni_{3.0}Co_{10}$AlBeta and Mi-$Ni_{3.0}Co_{10}$AlBeta zeolites were prepared by sequential impregnation of 2 g of mesoporous and microporous HAlBeta with an aqueous solution of $Co(NO_3)_2 \cdot 6\,H_2O$ at pH of 2.6–3.0 and a concentration of 10^{-2} mol L^{-1} and then with an aqueous solution of $Ni(NO_3)_2 \cdot 6\,H_2O$ at pH of 2.70–3.0 and a concentration of 10^{-3} mol L^{-1} under aerobic conditions. During sequential impregnation, the suspensions were stirred during 24 h at room temperature and the separation of the solids from the fraction of suspension was performed in an evaporator under the vacuum of a membrane pump for 2 h in air at 60 °C. After calcination at 500 °C for 3 h in air, the obtained zeolite catalysts containing 10 wt% of cobalt and 3.0 wt% of nickel were marked as Me-$Ni_{3.0}Co_{10}$AlBeta and Mi-$Ni_{3.0}Co_{10}$AlBeta, respectively. The Me-co-$Ni_{3.0}Co_{10}$AlBeta and Mi-co-$Ni_{3.0}Co_{10}$AlBeta zeolites were prepared by co-impregnation of 2 g of Me- and Mi-HAlBeta with an aqueous solutions containing both $Co(NO_3)_2 \cdot 6\,H_2O$ and $Ni(NO_3)_2 \cdot 6\,H_2O$ at pH of 2.70–3.0 under aerobic conditions in conditions similar to those described for the sequential one. After calcination at 500 °C for 3 h in air, the obtained zeolite catalysts containing 10 wt% of cobalt and 3.0 wt% of nickel were labelled as Me-co-$Ni_{3.0}Co_{10}$AlBeta and Mi-co-$Ni_{3.0}Co_{10}$AlBeta, respectively, where "co" stands for co-impregnation.

The second fraction of mesoporous and microporous TEABeta was treated with a 13 mol L^{-1} HNO_3 aqueous solution during 4 h at 80 °C to obtain dealuminated SiBeta with Si/Al of 490 for

mesoporous and Si/Al of 1516 for microporous supports, respectively. The Me-Ni$_{3.0}$Co$_{10}$SiBeta and Mi-Ni$_{3.0}$Co$_{10}$SiBeta zeolites were prepared by sequential impregnation of 2 g of mesoporous and microporous SiBeta with an aqueous solution of Co(NO$_3$)$_2$·6 H$_2$O at pH of 2.5–3.0 and a concentration of 10^{-2} mol L^{-1} and then with an aqueous solution of Ni(NO$_3$)$_2$·6 H$_2$O at pH = 2.6–3.0 and a concentration of 10^{-3} mol L^{-1} under aerobic conditions. After impregnation of Beta zeolite with Co(NO$_3$)$_2$·6 H$_2$O salt, the suspensions were stirred for 24 h at room temperature and then, the separation of the solids from the fraction of suspension was performed in an evaporator under the vacuum of a membrane pump for 2 h in air at 60 °C. Such prepared materials were impregnated by an aqueous solution of Ni(NO$_3$)$_2$·6 H$_2$O and the suspensions were stirred and evaporated in the same conditions once again. After calcination at 500 °C for 3 h in air, the obtained zeolite catalysts containing 10 wt% of cobalt and 3.0 wt% of nickel were labelled as Me-Ni$_{3.0}$Co$_{10}$SiBeta and Mi-Ni$_{3.0}$Co$_{10}$SiBeta, respectively. The Me-co-Ni$_{3.0}$Co$_{10}$SiBeta and Mi-co-Ni$_{3.0}$Co$_{10}$SiBeta zeolites were prepared by co-impregnation of 2 g of mesoporous and microporous SiBeta with an aqueous solutions of both Co(NO$_3$)$_2$·6 H$_2$O and Ni(NO$_3$)$_2$·6 H$_2$O at pH of 2.6–3.0 under aerobic conditions, in the conditions similar to that described for sequential one preparation. After calcination at 500 °C for 3 h in air the obtained zeolite catalysts containing 10 wt% of cobalt and 3.0 wt% of nickel were marked as Me-co-Ni$_{3.0}$Co$_{10}$SiBeta and Mi-co-Ni$_{3.0}$Co$_{10}$SiBeta, respectively.

Part of each obtained zeolite was reduced under atmospheric pressure in a flow of 5% H$_2$–95% Ar at 400 °C for 1 h to obtain zeolite catalysts, which were referred to as Red-Me-Ni$_{3.0}$Co$_{10}$AlBeta, Red-Mi-Ni$_{3.0}$Co$_{10}$AlBeta, Red-Me-co-Ni$_{3.0}$Co$_{10}$AlBeta, Red-Mi-co-Ni$_{3.0}$Co$_{10}$AlBeta, Red-Me-Ni$_{3.0}$Co$_{10}$SiBeta, Red-Mi-Ni$_{3.0}$Co$_{10}$SiBeta, Red-Me-co-Ni$_{3.0}$Co$_{10}$SiBeta, Red-Mi-co-Ni$_{3.0}$Co$_{10}$SiBeta, where "Red" stands for reduced.
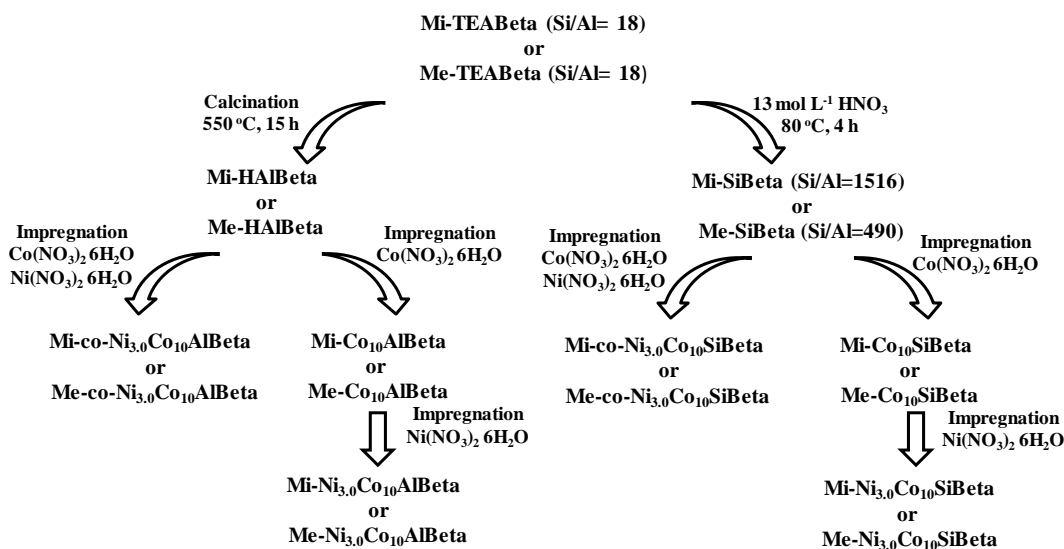
Scheme 1. Methods of preparation of mesoporous (marked as Me in Scheme 1) and microporous (marked as Mi in Scheme 1) NiCoBeta and co-NiCoBeta.

2.2. Characterization with Different Kinds of Techniques

2.2.1. XRD

The XRD patterns of nickel/cobalt-modified zeolite systems are shown in Figure 1. For all the samples, reflections at around 7.6° and 22.4° appear, which are characteristic of Beta zeolite and indicate the presence of two isomorphic forms of this material [8,26–28]. These studies show that the crystalline structure of Beta zeolite is preserved, even after the dealumination process and the incorporation of metals (Ni and Co) ions [29]. In case of all calcined NiCoBeta systems, the reflections characteristic of NiCo$_2$O$_4$ and/or Co$_3$O$_4$ are seen (2θ = 36.69°, 44.56°, 64.94°). The appearance of reflections at ca.

43.39° and 59.16° is associated with the presence of the NiO and Co_3O_4, respectively. Moreover, only for Me-$Ni_{3.0}Co_{10}$AlBeta and Mi-$Ni_{3.0}Co_{10}$SiBeta systems, the reflections related to NiO, Co_3O_4 and/or $NiCo_2O_4$ are observed [30–33].
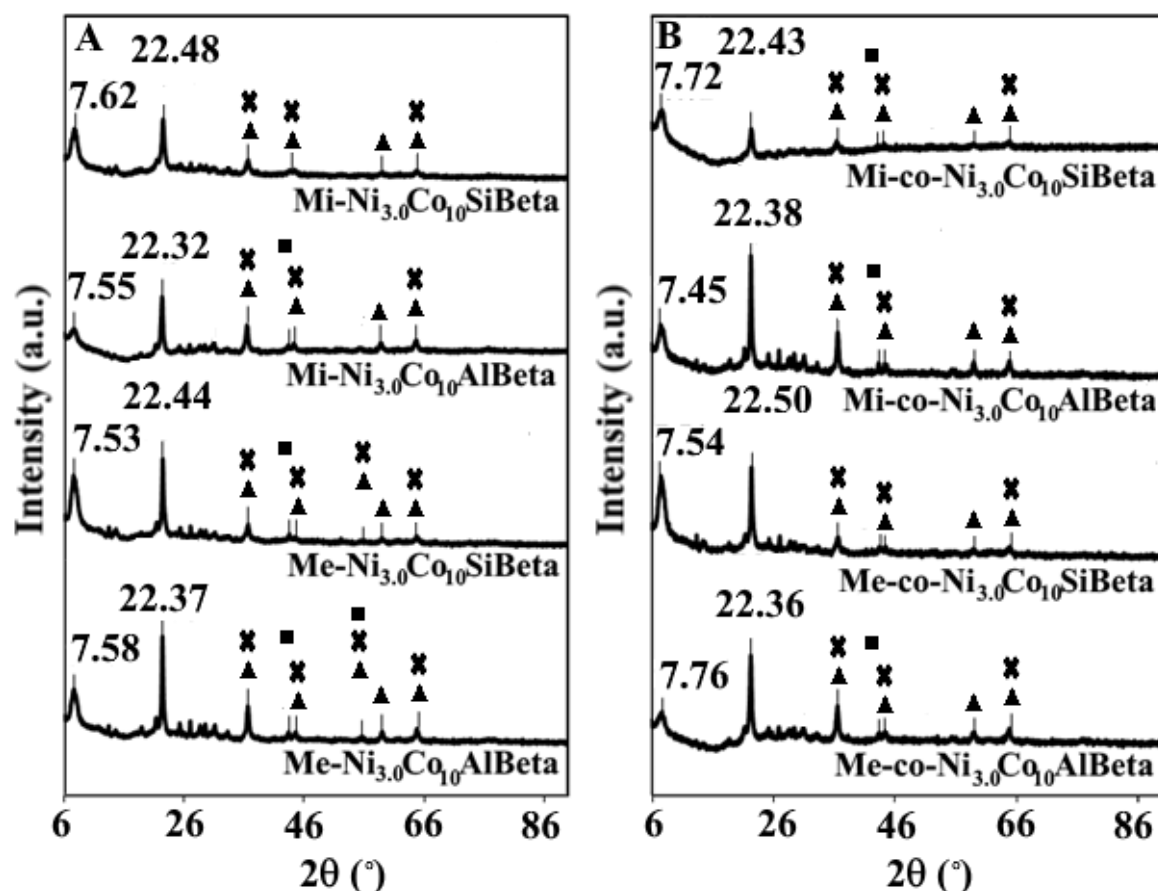

Figure 1. XRD patterns of (**A**) Me-$Ni_{3.0}Co_{10}$AlBeta, Mi-$Ni_{3.0}Co_{10}$AlBeta, Me-$Ni_{3.0}Co_{10}$SiBeta, Mi-$Ni_{3.0}Co_{10}$SiBeta and (**B**) Me-co-$Ni_{3.0}Co_{10}$AlBeta, Mi-co-$Ni_{3.0}Co_{10}$AlBeta, Me-co-$Ni_{3.0}Co_{10}$SiBeta, Mi-co-$Ni_{3.0}Co_{10}$SiBeta recorded at room temperature and ambient atmosphere (▲—Co_3O_4, ■—NiO, ✖—$NiCo_2O_4$).

After the hydrogen treatment of Mi-$Ni_{3.0}Co_{10}$Beta and Me-$Ni_{3.0}Co_{10}$Beta systems, the reflection related to the presence of Ni^0, Co^0 or/and Ni-Co alloy is seen ($2\theta = 44.41°$) (Figure 2) [31,34]. In case of Red-co-$Ni_{3.0}Co_{10}$Beta, one can observed reflections associated with the occurrence of Ni-Co alloy and/or metallic nickel and/or cobalt ($2\theta = 44.54°$). However, it can be noticed that the cobalt and nickel oxide phases are still visible ($2\theta = 36.54°$, 59.08° and 43.44°, respectively). Furthermore, for all co-impregnated systems, the reflection at ca. 65.06° is also shown, which may be related to the presence of Co_3O_4 or/and $NiCo_2O_4$ [30–34].
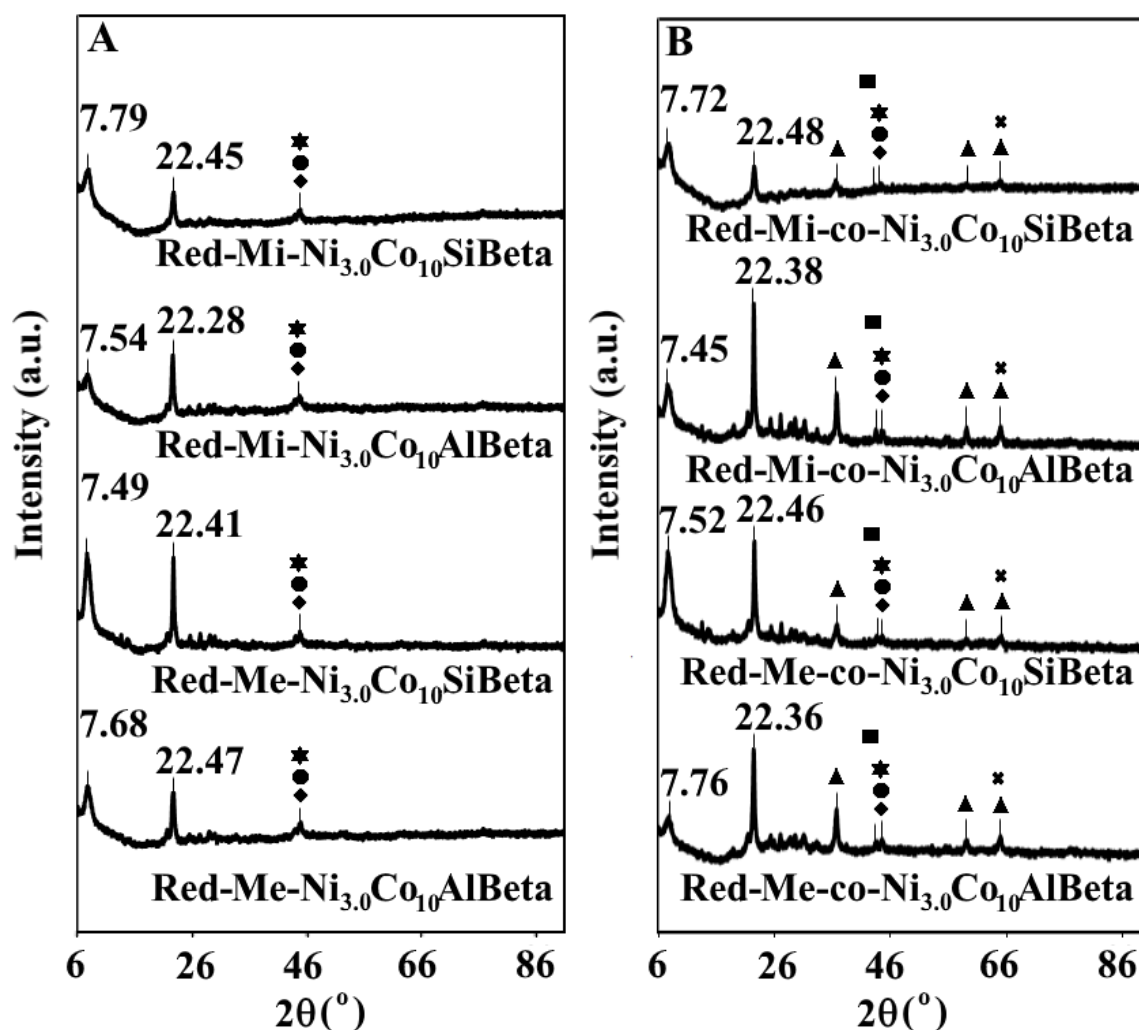
Figure 2. XRD patterns of (**A**) Red-Me-Ni$_{3.0}$Co$_{10}$AlBeta, Red-Mi-Ni$_{3.0}$Co$_{10}$AlBeta, Red-Me-Ni$_{3.0}$Co$_{10}$SiBeta, Red-Mi-Ni$_{3.0}$Co$_{10}$SiBeta and (**B**) Red-Me-co-Ni$_{3.0}$Co$_{10}$AlBeta, Red-Mi-co-Ni$_{3.0}$Co$_{10}$AlBeta, Red-Me-co-Ni$_{3.0}$Co$_{10}$SiBeta, Red-Mi-co-Ni$_{3.0}$Co$_{10}$SiBeta recorded at room temperature and ambient atmosphere (♦—Ni^0, ●—Co^0, ✱—Ni-Co alloy, ▲—Co$_3$O$_4$, ■—NiO, ✖—NiCo$_2$O$_4$).

2.2.2. XPS

The XPS analyzes of Ni$_{3.0}$Co$_{10}$Beta samples were performed for Si 2p, Al 2p, O 1s, C 1s, Ni 2p and Co 2p core lines.

Three doublets with the spin-orbit splitting of 0.61 eV were used to properly fit the Si 2p spectra. The porosity of zeolite matrix did not influence the relative intensities of these components. The most intense doublets (>93%) with Si 2p$_{3/2}$ BE values of 103.6–104.0 eV are associated with the presence of tetrahedral Si(IV) [35–37]. One can find that these values are somewhat larger than those reported for BEA, MFI and MOR zeolites earlier [38–42]. The much smaller low-BE component (Si 2p$_{3/2}$ BE of 101–102 eV) found in all the samples is distinctive for Si in lower than 4+ oxidation state. Such component can be related to the limited reduction of silicon under high-vacuum conditions or to the differential charging caused by some structural damages in the zeolite matrix.

The O 1s spectra are well decomposed into four components: (i) the most intense peak located at 533.0–533.7 eV referred to the lattice oxygen [43–45]; (ii) two peaks at 529.8–531.4 eV due to oxygen–metal bonds; (iii) a peak at BE higher than 534 eV assigned to OH groups, adsorbed water, and oxygen of organic contaminants. Careful analysis allows us to identify Co-O species with BE ~

529.9 eV and Ni-O species with BE ~ 531.2 eV (not shown here). This is in line with recent references found for $NiCo_2O_4$ (531.2 eV) [46], $Ni(OH)_2$ (531.1 eV) [47] and rock-salt type of structure of Co and Ni oxides (529.6 eV) [46].

Three peaks at 285.0 eV (organic contaminants), 286.0–286.2 eV (C-O groups) and > 289 eV (C=O groups) can be distinguished in the C 1s spectra. The binding energy of Al $2p_{3/2}$ core line is close to 75.0 eV, suggesting Al^{3+} (Al_2O_3 BE = 74.9 eV [48]).

Two nickel species with a relative intensities ratio close to 35:65 were identified in Ni 2p XPS spectra of all the zeolites under study. The minor components with lower BE of $2p_{3/2}$ region (854.4–854.8 eV) origin from the octahedral Ni^{2+} species were found in $NiCo_2O_4$ and $Ni(OH)_2$. The higher BE species (856.2–856.9 eV) are related to Ni^{3+} oxyhydroxides.

The Co 2p XPS results of microporous and mesoporous zeolites are presented in Figure 3A,B, respectively. The parameters obtained in the course of the numerical analysis are listed in Table 1. Well separated doublets (Co $2p_{3/2}$ and $2p_{1/2}$) are the result of strong spin-orbit coupling. The main peaks come from the charge-transfer (CT) states $2p^5 3d^8 L^{-1}$ (L—ligand), whereas respective shake-up satellites, which overlap the main lines, reflect non-CT $2p^5 3d^7$ states. The absolute BE values of the 2p peaks are not always sufficient in identifying the chemical environment of cobalt, since relatively small shifts are reported to. Some additional information helpful in such characterization can be achieved from the distance between two peaks in the doublet (spin-orbit splitting Δ_{SO}) and the satellite structure. The Co 2p doublets with Δ_{SO} of 15.1–15.9 eV and the occurrence of well-visible satellites uniquely identify the high-spin cobalt(II). One can find that except Me-$Ni_{3.0}Co_{10}$SiBeta, all spectra should be fitted with two main lines and associated satellites.

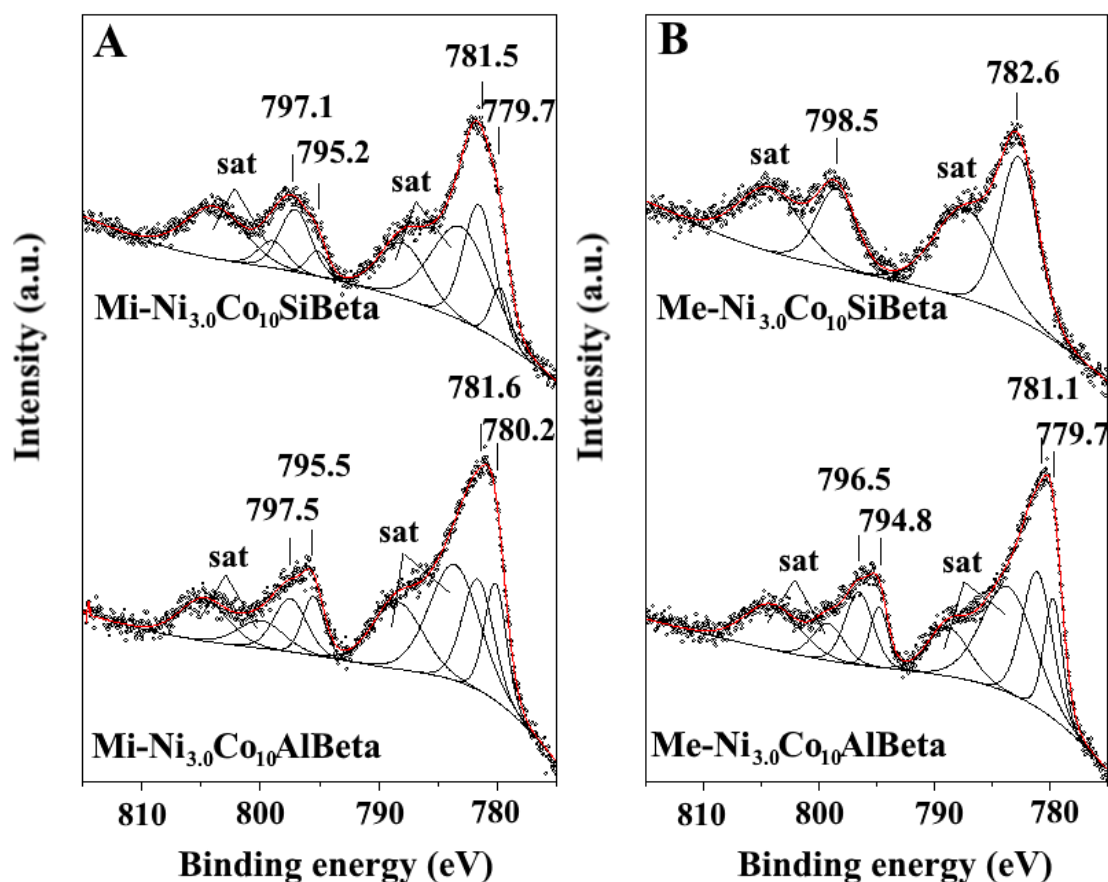**Figure 3.** Co 2p XPS spectra of (**A**) Mi-$Ni_{3.0}Co_{10}$SiBeta and Mi-$Ni_{3.0}Co_{10}$AlBeta and (**B**) Me-$Ni_{3.0}Co_{10}$SiBeta and Me-$Ni_{3.0}Co_{10}$AlBeta.

Table 1. The binding energies (eV) and relative areas of components (%) of Co $2p_{3/2}$ lines obtained for meso- and microporous samples. The spin-orbit splitting Δ_{SO} (eV) of each doublet is also listed.

Sample	A	B	Δ_{SO}	Satellites
Mi-Ni$_{3.0}$Co$_{10}$AlBeta	780.2	781.6	15.4–15.8	783.6–788.4
-	(42.6)	(57.4)	-	-
Mi-Ni$_{3.0}$Co$_{10}$SiBeta	779.7	781.5	15.4–15.5	783.1–788.0
-	(20.5)	(79.5)	-	-
Me-Ni$_{3.0}$Co$_{10}$AlBeta	779.7	781.0	15.1–15.5	783.6–788.7
-	(35.3)	(64.7)	-	-
Me-Ni$_{3.0}$Co$_{10}$SiBeta	-	782.6	15.9	787.3
-	-	(100)	-	-

The dominant component with Co $2p_{3/2}$ BE in the range of 781.0–781.6 eV is assigned to the tetrahedral Co(II) species embedded into the zeolite matrix. Minor components found in both microporous samples and Me-Ni$_{3.0}$Co$_{10}$AlBeta have Co $2p_{3/2}$ BE values in the range of 779.7–780.2 eV, which suggests Co(II) species in octahedral surroundings. Taking into account that the following values were reported: 780.0–780.3 eV for Co(OH)O, 780.0–780.9 eV for CoO, and 779.4–780.1 eV for Co$_3$O$_4$ [48–50], one can identify these components as the extra-framework oxides. It is worth mentioning that Me-Ni$_{3.0}$Co$_{10}$SiBeta zeolite shows only one broad component with very high Co $2p_{3/2}$ BE of 782.6 eV, which suggests octahedral Co(III) species in the low-spin configuration [51]. However, the most intense satellite structure was also found in this sample, which is in contrast to the expected weakening of the satellite structure in low-spin cobalt(III) component [52]. On the other hand, similar high BE values of Co species were observed for several zeolites, recently [53–56]. Many metal cations (e.g., Fe, Cr, Cu) embedded in zeolites often show higher BE comparing to their BE in oxides [36,57,58]. This may be due to the degree of cations dispersion as well as the nature of their interactions with the zeolite matrix. Thus, the higher BE of Co(II) might be the manifestation of highly isolated species in our sample. All these findings make Me-Ni$_{3.0}$Co$_{10}$SiBeta unique among all the measured samples.

2.2.3. NH$_3$-TPD

The NH$_3$-TPD of metals-modified samples are presented in Figure 4. The position of two unresolved peaks with maxima at ca. 220 and 450 °C are described to Lewis and Brønsted acidic sites, respectively, in agreement with earlier report [59]. For co-Ni$_{3.0}$Co$_{10}$SiBeta and Ni$_{3.0}$Co$_{10}$SiBeta, one can see the shift of both maxima to lower temperatures. This could be assigned to the presence of lower strength Lewis acidic sites and the removal of the strong Brønsted acidic sites during the dealumination process, respectively [14]. The removal of the aluminum leads also to the decrease of the intensity of above-mentioned peaks, which is quite well seen in the case of the Ni$_{3.0}$Co$_{10}$SiBeta samples. Furthermore, for dealuminated systems, the position of peak at ca. 224 °C (for Me-Ni$_{3.0}$Co$_{10}$AlBeta), 246 °C (for Mi-Ni$_{3.0}$Co$_{10}$AlBeta), 222 °C (for Me-co-Ni$_{3.0}$Co$_{10}$AlBeta) and 227 °C (for Mi-co-Ni$_{3.0}$Co$_{10}$AlBeta) shifted to 213 °C (for Me-Ni$_{3.0}$Co$_{10}$SiBeta), 207 °C (for Mi-Ni$_{3.0}$Co$_{10}$SiBeta), 211 °C (for Me-Ni$_{3.0}$Co$_{10}$SiBeta) and 209 °C (for Mi-co-Ni$_{3.0}$Co$_{10}$SiBeta), respectively. This phenomenon suggests that the latter samples contain, in their structure, Lewis acidic sites with lower strength, as compared to corresponding non-dealuminated systems. Moreover, the presence of nickel causes the shift to higher temperatures of low-temperature peak, as compared to Co-based catalysts [25].

In case of reduced catalysts (Figure 5), peaks at ca. 210 and 440 °C were observed, which are related to Lewis and Brønsted acidic sites, respectively [59]. It should be noted that the reduction of co-NiCoBeta and NiCoBeta systems resulted in the enhancement of a high temperature peak intensity. The same phenomenon was observed by Stanton et al., who associated it with the formation of metal acid sites [60].
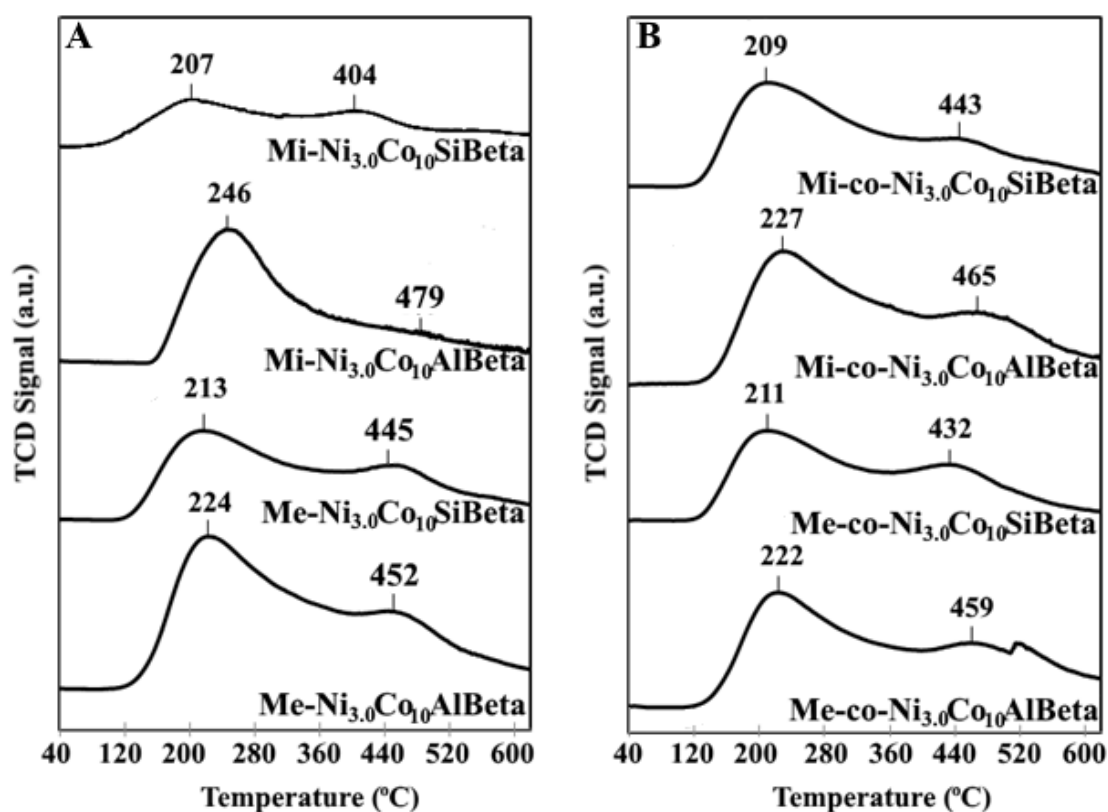
Figure 4. NH$_3$-TPD profiles of (**A**) Me-Ni$_{3.0}$Co$_{10}$Beta, Mi-Ni$_{3.0}$Co$_{10}$Beta and (**B**) Me-co-Ni$_{3.0}$Co$_{10}$Beta, Mi-co-Ni$_{3.0}$Co$_{10}$Beta.
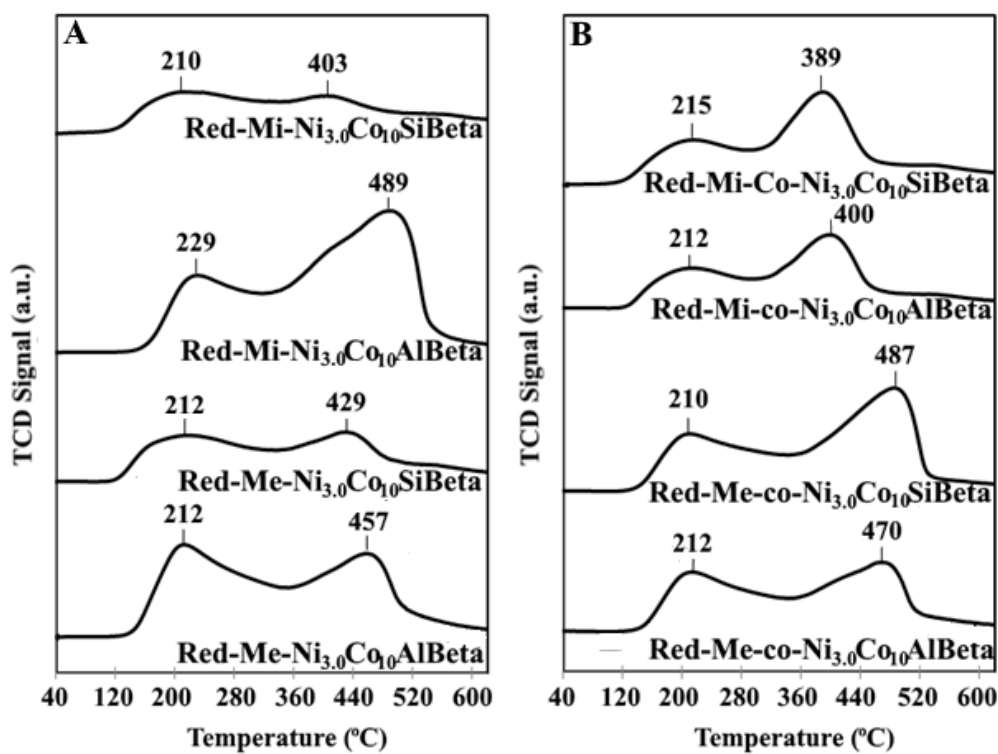
Figure 5. NH$_3$-TPD profiles of (**A**) Red-Me-Ni$_{3.0}$Co$_{10}$Beta, Red-Mi-Ni$_{3.0}$Co$_{10}$Beta and (**B**) Red-Me-co-Ni$_{3.0}$Co$_{10}$Beta, Red-Mi-co-Ni$_{3.0}$Co$_{10}$Beta.

As shown in Table 2, the dealumination of nickel-cobalt based systems led to a decrease in their acidity. This is the result of the removal of aluminum from the framework of these materials [14]. A comparison of the NH_3-TPD results for the previously tested CoBeta zeolite samples [14] with those presented in this paper $Ni_{3.0}Co_{10}$Beta systems allows to conclude that the addition of nickel to cobalt-based samples causes a change in their acidity. For Mi-co-$Ni_{3.0}Co_{10}$AlBeta and Me-$Ni_{3.0}Co_{10}$AlBeta, the introduction of this metal increases the amount of adsorbed NH_3. This may be associated with the creation of additional adsorption centres. In other cases, the presence of the Ni decreased the acidity of the CoBeta systems, which is probably related to the blockage of acidic sites by nickel oxides [14]. However, the reduction of tested systems led to the increase of their acidity.

Table 2. The quantitative data of NH_3-TPD for reduced and non-reduced $Ni_{3.0}Co_{10}$Beta systems.

Sample	a_{NH3} (μmol g^{-1})	Sample *	a_{NH3} (μmol g^{-1}) *
Mi-$Ni_{3.0}Co_{10}$AlBeta	1006	Mi-HAlBeta	1459
Red-Mi-$Ni_{3.0}Co_{10}$AlBeta	2914	Mi-Co_{10}AlBeta	1404
Mi-co-$Ni_{3.0}Co_{10}$AlBeta	1586	Red-Mi-Co_{10}AlBeta	2555
Red-Mi-co-$Ni_{3.0}Co_{10}$AlBeta	2604	-	-
Mi-$Ni_{3.0}Co_{10}$SiBeta	590	Mi-SiBeta	435
Red-Mi-$Ni_{3.0}Co_{10}$SiBeta	1048	Mi-Co_{10}SiBeta	1430
Mi-co-$Ni_{3.0}Co_{10}$SiBeta	1265	Red-Mi-Co_{10}SiBeta	1350
Red-Mi-co-$Ni_{3.0}Co_{10}$SiBeta	1986	-	-
Me-$Ni_{3.0}Co_{10}$AlBeta	1598	Me-HAlBeta	1488
Red-Me-$Ni_{3.0}Co_{10}$AlBeta	2179	Me-Co_{10}AlBeta	1404
Me-co-$Ni_{3.0}Co_{10}$AlBeta	1364	Red-Me-Co_{10}AlBeta	2569
Red-Me-co-$Ni_{3.0}Co_{10}$AlBeta	2103	-	-
Me-$Ni_{3.0}Co_{10}$SiBeta	947	Me-SiBeta	419
Red-Me-$Ni_{3.0}Co_{10}$SiBeta	1389	Me-Co_{10}SiBeta	1358
Me-co-$Ni_{3.0}Co_{10}$SiBeta	1161	Red-Me-Co_{10}SiBeta	1130
Red-Me-co-$Ni_{3.0}Co_{10}$SiBeta	1710	-	-

* The data from ref. [26].

2.2.4. H_2-TPR

Figure 6 shows H_2-TPR profiles for all the tested samples, which exhibit peaks in the temperature range of 266–394 °C. The first peak with the maximum at 266–296 °C may be related to the reduction of Co_3O_4 and/or bulk NiO in the extra-framework positions to CoO and Ni^0, respectively. Furthermore, one can observe the peaks with the maximum in the temperature range of 304–394 °C. Their presence is related to the reduction of CoO and/or octahedral Ni(II) species [14,28,61,62]. As compared to previous studies on cobalt-modified Beta zeolite, the small addition of nickel to zeolite cobalt systems leads to a decrease in the reduction temperature of cobalt oxides present outside of the zeolite network by about 50 °C. A similar influence of nickel on the reducibility of alumina supported cobalt systems was observed by Rytter et al. [24]. The authors claimed that the lowering of reduction temperature can be related to the spillover of the hydrogen from the metallic nickel particles to cobalt oxides. Moreover, it has also been suggested that the reduction profiles of the tested samples may be associated with the formation of solid solution between various oxide phases of Co, Ni and the support. As one can see, only for dealuminated samples, a peak above 700 °C is also seen. Its appearance can be attributed to the reduction of hardly reducible Co species (cobalt aluminate or/and cobalt silicates) and/or pseudo-tetrahedral ions of Co(II), which are located in the vacant T-atom sites created as a result of dealumination [14,32,63].
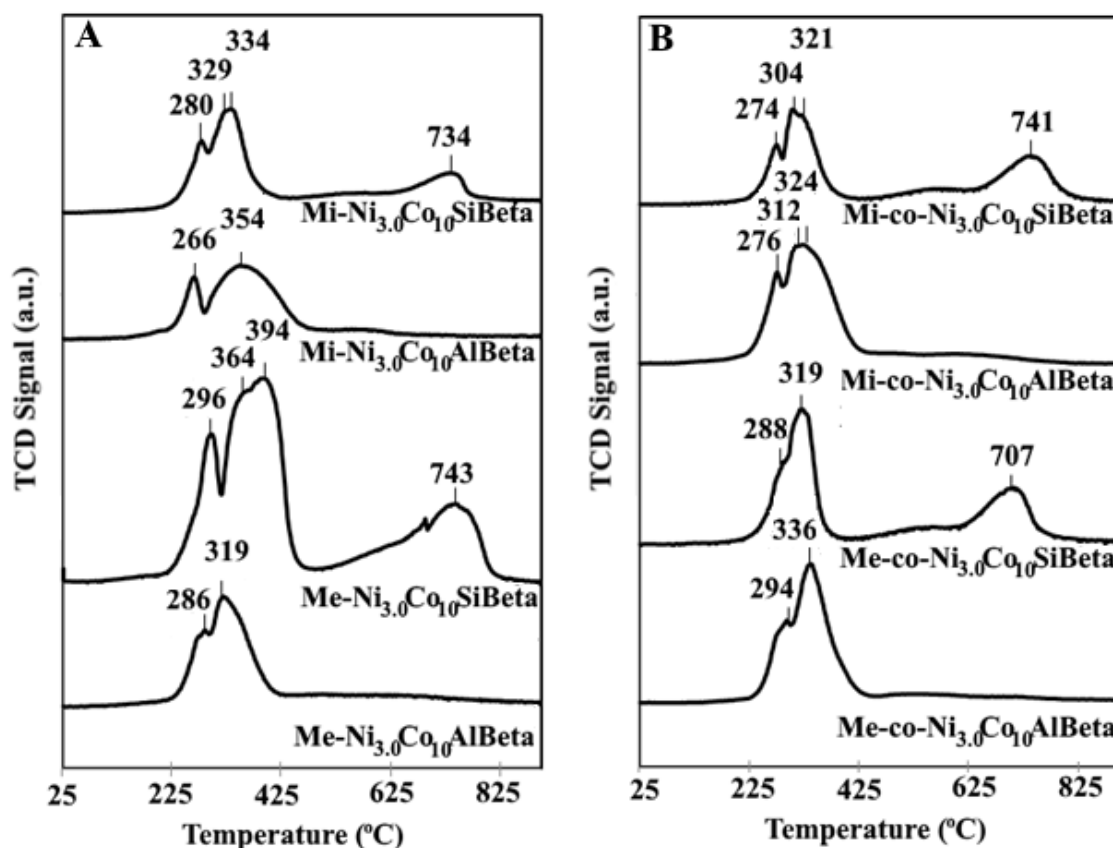
Figure 6. TPR-H$_2$ profiles of (**A**) Me-Ni$_{3.0}$Co$_{10}$Beta, Mi-Ni$_{3.0}$Co$_{10}$Beta and (**B**) Me-co-Ni$_{3.0}$Co$_{10}$Beta, Mi-co-Ni$_{3.0}$Co$_{10}$Beta.

2.2.5. TEM EDX

TEM observations and analysis were carried out for the reduced Ni$_{3.0}$Co$_{10}$Beta and co-Ni$_{3.0}$Co$_{10}$Beta samples. The bright field TEM micrographs reported in Figure 7A illustrate the dispersion of the nanoparticles on the supports with a large repartition of diameters: from a few nm to 100 nm.

X-ray Energy Dispersive Spectroscopy was carried out with 1 nm electron probe in order to analyze the chemical composition of nanoparticles. Twenty nanoparticles were analyzed for each sample. The representative EDS spectra are reported in Figure 7B for each sample. It should be noted that Cu peaks are present in all spectra because of the presence of this metal in the grids used in the experiment. Both peaks of Co and Ni were observed on all recorded spectra. The average Co and Ni content (atomic %) is 80 and 20 for all measured samples. Thus, the chemical composition of the nanoparticles is similar for all of the catalysts under study and close to the nominal Co/Ni ratio of 3.0.

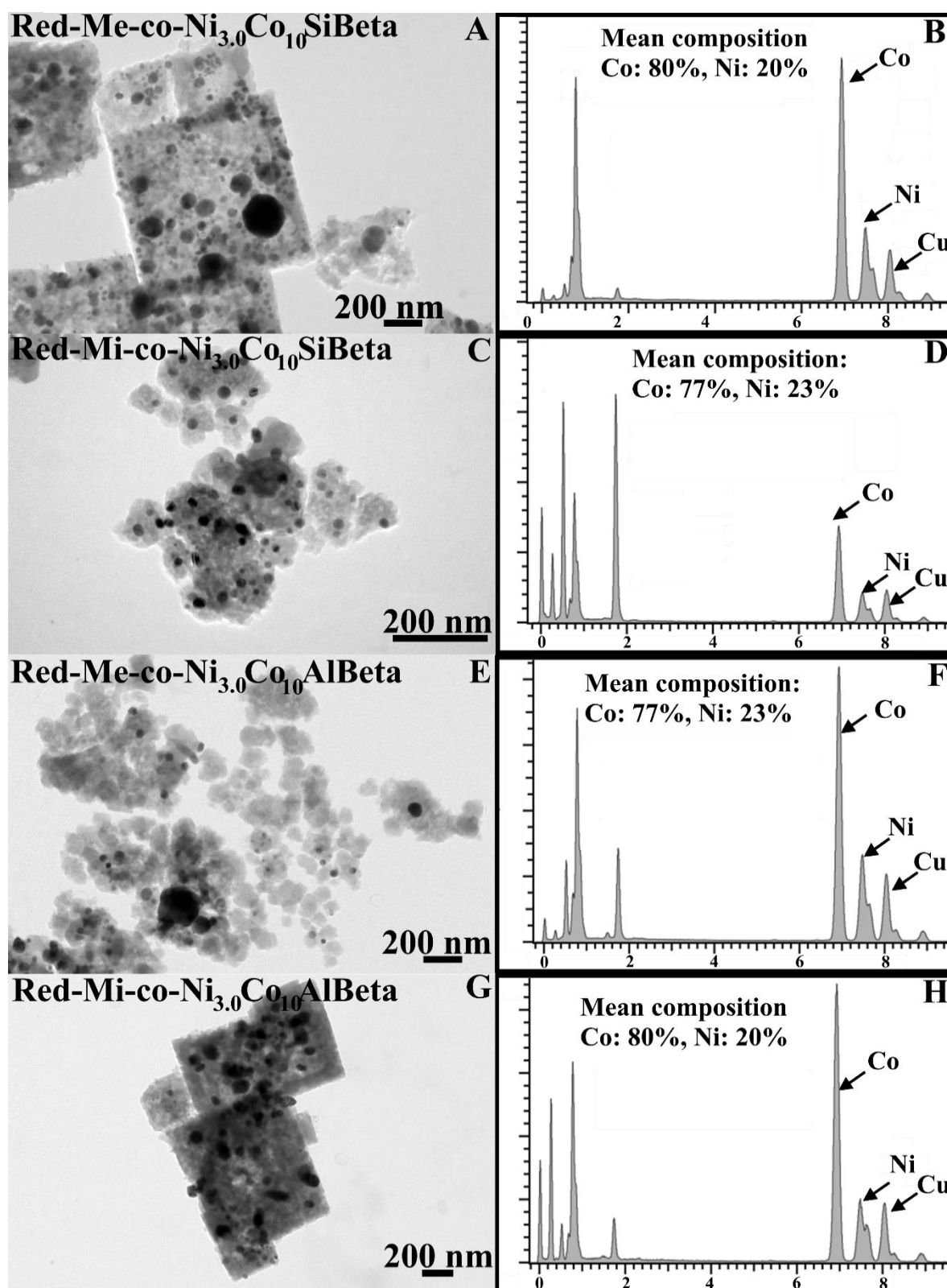**Figure 7.** TEM bright field micrographs (**A**,**C**,**E**,**G**) with a representative EDS spectra (**B**,**D**,**F**,**H**) of Red-Me-co-Ni$_{3.0}$Co$_{10}$SiBeta, Red-Mi-co-Ni$_{3.0}$Co$_{10}$SiBeta, Red-Me-co-Ni$_{3.0}$Co$_{10}$AlBeta, Red-Mi-co-Ni$_{3.0}$Co$_{10}$AlBeta.

2.3. Fischer–Tropsch Synthesis

The activity and selectivity to liquid products of FTS catalysts can be modified by the use of different secondary metals, e.g., transition or noble metals [1,2]. Thus, we focused our study on the correlation between the active phase (Co species) of the catalysts and the addition (Ni) and its impact on the process flow. The CO conversion and selectivity to C_1-C_4, CO_2, and liquid products for Red-NiCoBeta and Red-co-NiCoBeta systems are summarized in Table 3 and in Figures 8 and 9, respectively.

Table 3. The catalytic activity and selectivity of tested samples in Fischer–Tropsch synthesis.

Sample	CO Conversion (%)	Selectivity Towards (%)			Iso/n-Alkane Ratio	Alcohols/ Alkane Ratio	Unsaturated/ Alkane Ratio	α C_1-C_4
		C_1-C_4	CO_2	Liquid Products				
Red-Mi-Ni$_{3.0}$Co$_{10}$AlBeta	95.19	16.58	6.72	76.70	2.26	0.26	0.74	0.86
Red-Mi-co-Ni$_{3.0}$Co$_{10}$AlBeta	17.02	4.08	0.00	95.92	2.62	0.12	0.39	0.59
Red-Mi-Ni$_{3.0}$Co$_{10}$SiBeta	99.68	17.97	6.47	75.56	3.12	0.00	2.98	0.32
Red-Mi-co-Ni$_{3.0}$Co$_{10}$SiBeta	99.66	18.19	6.50	75.31	1.18	0.00	0.15	0.65
Red-Me-Ni$_{3.0}$Co$_{10}$AlBeta	16.45	0.00	0.00	100.00	2.44	0.29	0.21	0.53
Red-Me-co-Ni$_{3.0}$Co$_{10}$AlBeta	17.29	1.05	0.00	98.95	1.22	0.00	0.17	0.64
Red-Me-Ni$_{3.0}$Co$_{10}$SiBeta	81.46	12.38	0.00	87.62	1.58	0.16	0.48	0.84
Red-Me-co-Ni$_{3.0}$Co$_{10}$SiBeta	97.86	16.94	6.48	76.58	0.91	0.17	0.18	0.80

Figure 8. Conversion of CO (▢) and selectivity to C_1-C_4 (▤), CO_2 (▨) and liquid products (■) after Fischer–Tropsch synthesis (T = 260 °C, p = 30 atm, t = 24 h) over (**A**) Red-Mi-Ni$_{3.0}$Co$_{10}$AlBeta, (**B**) Red-Me-Ni$_{3.0}$Co$_{10}$AlBeta, (**C**) Red-Mi-Ni$_{3.0}$Co$_{10}$SiBeta, (**D**) Red-Me-Ni$_{3.0}$Co$_{10}$SiBeta.
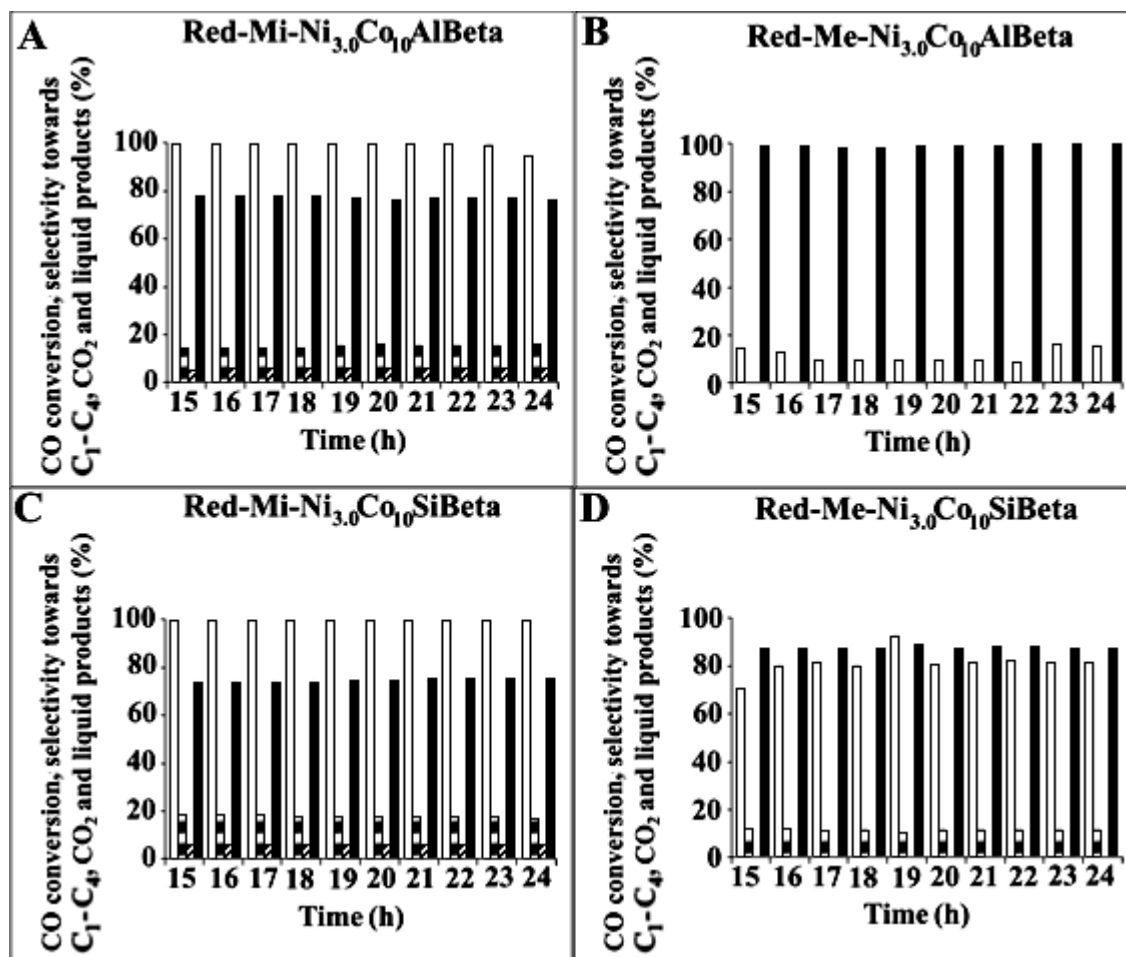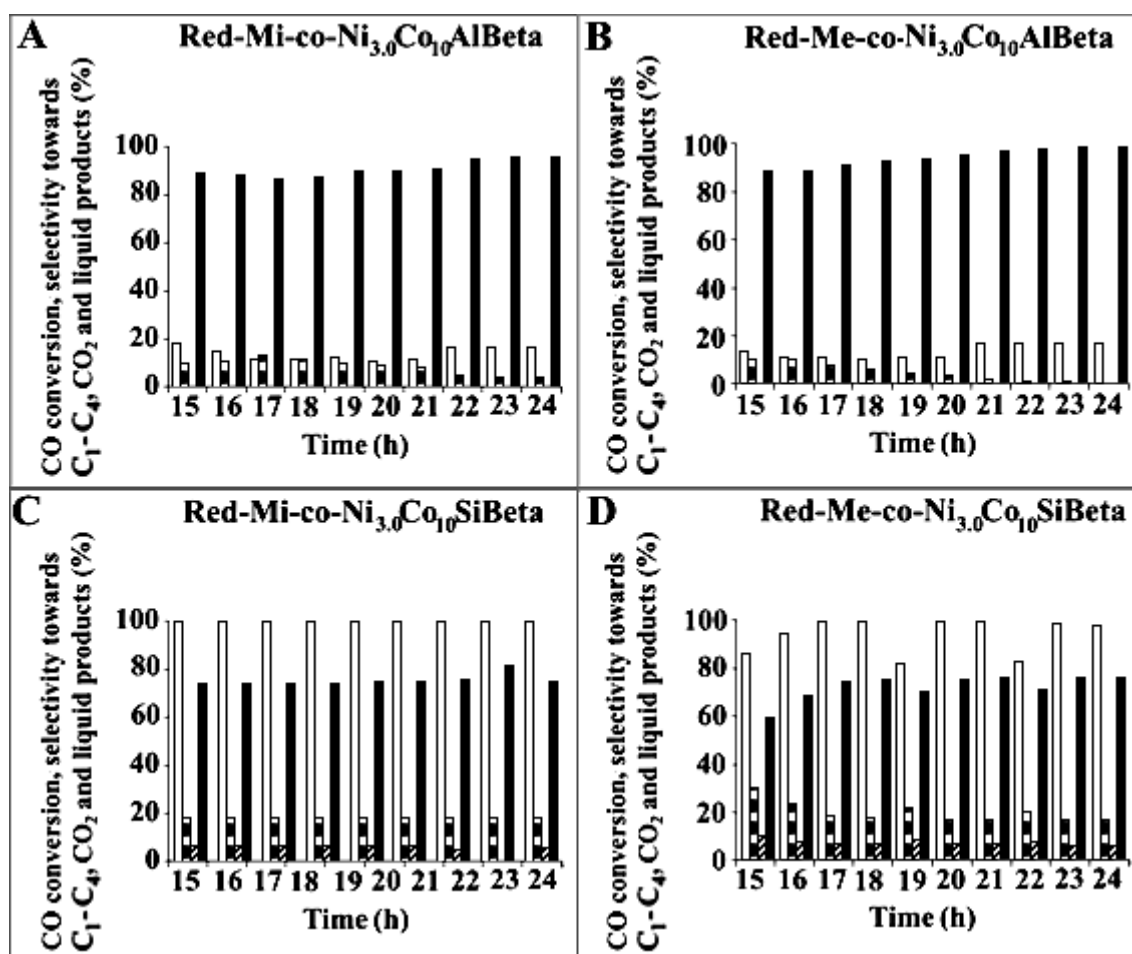
Figure 9. Conversion of CO (□) and selectivity to C_1-C_4 (▤), CO_2 (▧) and liquid products (■) after Fischer-Tropsch synthesis (T = 260 °C, p = 30 atm, t = 24 h) over (**A**) Red-Mi-co-$Ni_{3.0}Co_{10}$AlBeta, (**B**) Red-Me-co-$Ni_{3.0}Co_{10}$AlBeta, (**C**) Red-Mi-co-$Ni_{3.0}Co_{10}$SiBeta, (**D**) Red-Me-co-$Ni_{3.0}Co_{10}$SiBeta.

Among the reduced catalysts, the most active were the dealuminated ones. Red-Mi-$Ni_{3.0}Co_{10}$SiBeta and Red-Me-$Ni_{3.0}Co_{10}$SiBeta catalysts, prepared by sequential impregnation, exhibit not only high CO conversion (81–97%) but also better selectivity to liquid products of 88% and 75%, respectively. The catalytic behavior of Red-Mi-$Ni_{3.0}Co_{10}$AlBeta is very similar to that of Red-Mi-$Ni_{3.0}Co_{10}$SiBeta and shows the conversion of CO and liquid products selectivity equal to 95% and 77%, respectively. Catalytic properties of Red-Me-$Ni_{3.0}Co_{10}$AlBeta are quite unique because it exhibits much lower CO conversion (16%), but higher selectivity towards liquid products (100%).

Like in the case of samples obtained by sequential impregnation, the most active catalysts, prepared by co-impregnation are dealuminated systems (Red-Mi-co-$Ni_{3.0}Co_{10}$SiBeta and Red-Me-co-$Ni_{3.0}Co_{10}$SiBeta). They show very high CO conversion of about 98–100% and selectivity to liquid products of ca. 75–77%. Both Red-Mi-co-$Ni_{3.0}Co_{10}$AlBeta and Red-Me-co-$Ni_{3.0}Co_{10}$AlBeta exhibit a lower CO conversion (17%), but a higher liquid hydrocarbon selectivity (96–99%). It is worth mentioning that all samples, except Red-Me-$Ni_{3.0}Co_{10}$SiBeta, exhibit higher CO conversion than Co-based systems [25,64]. A similar conclusion was reported by Wang et al. for Ru, Ni promoted Co/HZSM-5 catalysts [2]. They related this phenomenon to the improvement of the CO hydrogenation by increasing the amount of available Co^0 active sites. Furthermore, in case of Red-Mi-co-$Ni_{3.0}Co_{10}$SiBeta and Red-Me-co-$Ni_{3.0}Co_{10}$SiBeta, the selectivity towards carbon dioxide is quite stable during the time of synthesis and is about 6.5% for all these catalysts. The addition of nickel hinders the selectivity to liquid products, but increases the selectivity to C_1-C_4, which can be

related to the good ability of this metal to break C-C bonds [2]. The same tendency was observed by Shimura et al. over Ru, Ni promoted Co/HZSM-5 catalysts [65]. Moreover, for microporous catalysts the selectivity to C_1-C_4 (4–18%) was higher than for corresponding mesoporous samples (0–17%). This is most likely due to CO diffusion limitation because of high H_2 to CO ratio on the catalyst surface. Our results are consistent with earlier studies on Co-containing microporous and mesoporous Beta zeolite catalysts [25].

The catalytic activity of all tested NiCoBeta and co-NiCoBeta catalysts remained stable throughout the duration of the FTS. According to Ritter et al. [24], the high stability of nickel-cobalt based catalysts may be due to the hydrogen spillover from metallic nickel particles to cobalt oxides, which decreases re-oxidation of the active phase, sintering and the creation of the carbon deposition on the catalyst surface. Furthermore, the authors also pointed out that the presence of Ni on the surface of cobalt-based system could obstruct the formation of graphitic carbon, which can also delay the deactivation of the catalyst.

The gas chromatography with mass spectroscopy (GC-MS) analysis of liquid products formed in FTS is presented in Table 3 and Figures 10 and 11. The research show that the presence of only micropores in the structure of Beta zeolite led to the production of C_7-C_{21} iso- and n-alkanes. However, as it was demonstrated, the nickel-cobalt based catalysts supported on the zeolitic mesoporous materials exhibited the creation of C_7-C_{21} isoalkanes and saturated hydrocarbons. The Red-Mi-$Ni_{3.0}Co_{10}$Beta catalyst exhibited a higher isoalkanes/n-alkanes ratio (≥1.18) than the corresponding Red-Me-$Ni_{3.0}Co_{10}$Beta catalyst (≥0.91). As compared to Red-Co-base catalysts [25], it can be seen that the addition of Ni resulted in the decrease of the selectivity towards isoalkanes, which is in the contrast to the results presented by Wang et al. [2], who observed the opposite trend. Furthermore, the correlation between the preparation method and the selectivity towards isoalkanes is hard to define. For Red-Mi-co-$Ni_{3.0}Co_{10}$AlBeta, Red-Me-$Ni_{3.0}Co_{10}$AlBeta and Red-Me-co-$Ni_{3.0}Co_{10}$AlBeta, the isoalkanes to n-alkanes ratio (2.62, 2.44 and 1.22, respectively) was higher than for corresponding dealuminated samples (1.18, 1.58 and 0.91, respectively). In case of Red-Mi-$Ni_{3.0}Co_{10}$AlBeta and Red-Mi-$Ni_{3.0}Co_{10}$SiBeta, the opposite tendency was observed. It should be noted that for all Ni and Co containing catalysts, the formation of unsaturated hydrocarbons was seen and the ratio of unsaturated to saturated hydrocarbons depends on the preparation method. The catalysts obtained by sequential impregnation exhibited higher unsaturated/n-alkanes ratio (≥0.21) than Red-co-NiCoBeta systems (≥0.15). Moreover, in the case of the Red-Me-$Ni_{3.0}Co_{10}$Beta, one can observe a more diverse distribution of the liquid products. For the dealuminated samples, except Red-Mi-co-$Ni_{3.0}Co_{10}$AlBeta, we observed a similar phenomenon as Martinez and Lopez over hybrid H-ZSM-5 catalysts [11], namely the higher formation of oxygenates by dealuminated systems. The main reason for the differences in the obtained liquid products in FTS is the presence of two kinds of acidic centers on the surface of the Red-$Ni_{3.0}Co_{10}$AlBeta (Red-co-$Ni_{3.0}Co_{10}$AlBeta) and Red-$Ni_{3.0}Co_{10}$SiBeta (Red-co-$Ni_{3.0}Co_{10}$SiBeta) systems.

In Table 4, the estimation of the total amount of all products per gram of catalysts is shown. These calculation are in line with results of CO conversion and products selectivity. The highest amount of products was noted for microporous cobalt Beta zeolites—Red-Mi-$Ni_{3.0}Co_{10}$SiBeta and Red-Mi-co-$Ni_{3.0}Co_{10}$SiBeta catalysts that also showed the highest activity in FTS process. It is also worth noting that in the case of Red-Mi-$Ni_{3.0}Co_{10}$AlBeta, the amount of all products after stabilization time of catalysts (15 h) is very small, but with the time reaction rising, the amount of formed product increases significantly. In the case of mesoporous cobalt silica Beta zeolites—Red-Me-$Ni_{3.0}Co_{10}$SiBeta and Red-Me-co-$Ni_{3.0}Co_{10}$SiBeta—despite of their high activity and similar CO conversion to microporous catalysts, the total amount of all products is smaller.
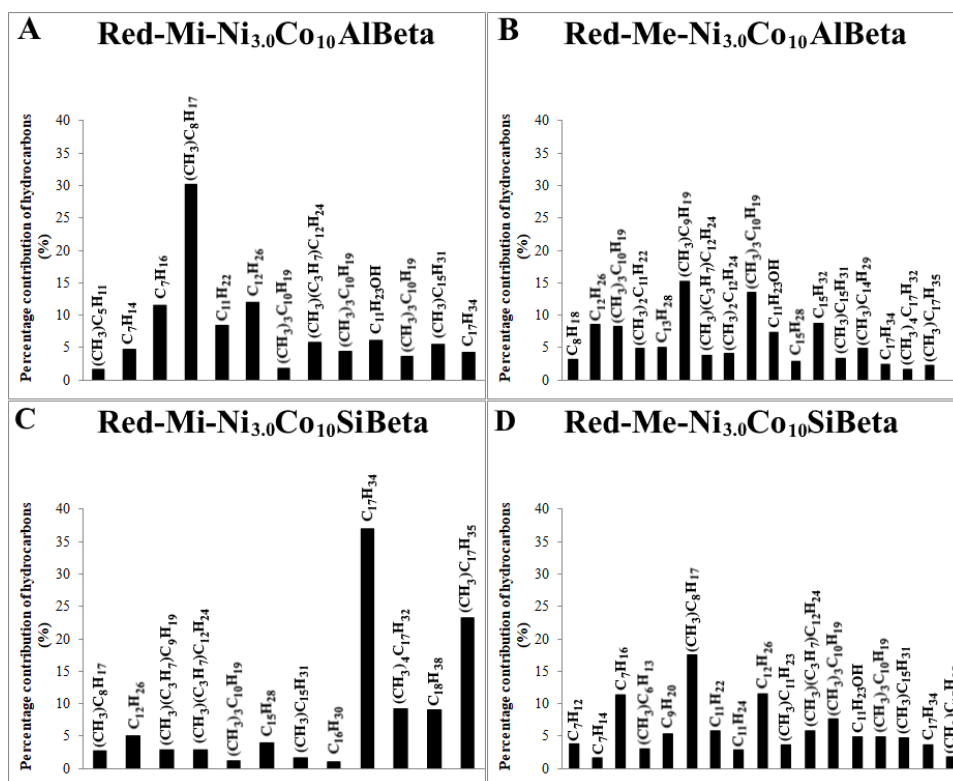
Figure 10. GC–MS analysis of liquid products achieved in FTS over (**A**) Red-Mi-Ni$_{3.0}$Co$_{10}$AlBeta, (**B**) Red-Me-Ni$_{3.0}$Co$_{10}$AlBeta, (**C**) Red-Mi-Ni$_{3.0}$Co$_{10}$SiBeta, (**D**) Red-Me-Ni$_{3.0}$Co$_{10}$SiBeta.
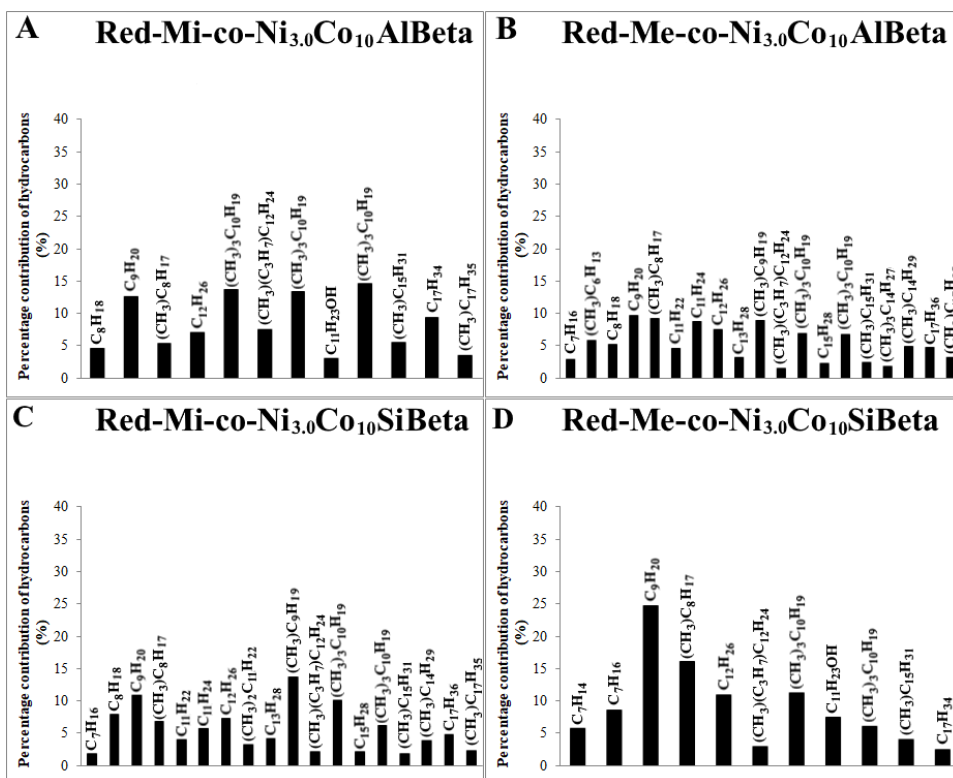
Figure 11. GC-MS analysis of liquid products achieved in FTS over (**A**) Red-Mi-co-Ni$_{3.0}$Co$_{10}$AlBeta, (**B**) Red-Me-co-Ni$_{3.0}$Co$_{10}$AlBeta, (**C**) Red-Mi-co-Ni$_{3.0}$Co$_{10}$SiBeta, (**D**) Red-Me-co-Ni$_{3.0}$Co$_{10}$SiBeta.

Table 4. The total amount of all products (millimole per gram of catalysts) calculated on the base of carbon balance data and CO conversion.

Catalyst	Reaction Time (h)	The Total Amount of All Products (Millimole/$g_{cat.}$)
Red-Mi-Ni$_{3.0}$Co$_{10}$AlBeta	15	0.002
	24	1.564
Red-Mi-co-Ni$_{3.0}$Co$_{10}$AlBeta	15	0.31
	24	0.28
Red-Mi-Ni$_{3.0}$Co$_{10}$SiBeta	15	1.638
	24	1.636
Red-Mi-co-Ni$_{3.0}$Co$_{10}$SiBeta	15	1.528
	24	1.636
Red-Me-Ni$_{3.0}$Co$_{10}$AlBeta	15	0.248
	24	0.27
Red-Me-co-Ni$_{3.0}$Co$_{10}$AlBeta	15	0.238
	24	0.284
Red-Me-Ni$_{3.0}$Co$_{10}$SiBeta	15	1.17
	24	1.338
Red-Me-co-Ni$_{3.0}$Co$_{10}$SiBeta	15	1.406
	24	1.606

The chain growth probability (α) of FTS liquid products for all systems was determined through the use of the Anderson-Schultz-Flory distribution (Table 3). According to Cheng et al. [66], the high value of chain growth probability is connected with a small olefin to paraffin ratio. However, in our work, we did not observe such a tendency. The value of α for C$_{5+}$ selectivity for co-NiCoBeta and NiCoBeta systems is in the range of 0.76–1.11. The microporous catalysts exhibit a higher chain growth probability value than mesoporous ones. A similar dependency was observed for Co zeolite catalysts in our earlier works [25,64]. The chain growth probability for the gaseous product of the FTS (α for C$_1$-C$_4$ selectivity) for all samples, except Red-Ni$_{3.0}$Co$_{10}$AlBeta and Red-Ni$_{3.0}$Co$_{10}$SiBeta, shows the opposite tendency than α for C$_{5+}$ selectivity. In Table 4, the gaseous products carbon balance after 15 and 24 h of reaction is shown.

In order to support the formation of the products via hydrogenation process of CO, Fourier Transform Infrared Spectroscopy (FT-IR) measurements of the liquid products were performed and the results are given in Figure 12. FT-IR spectra recorded for all samples present characteristic IR band located at 3300 cm^{-1} assigned to the -OH groups forming hydrogen bonds or the -OH groups occurring in alcohols [67]. The characteristic bands visible in the range of 2850–2980 cm^{-1} are attributed to the stretching vibration of C-H in aliphatic hydrocarbons, respectively, while the IR bands at 1016, 1000 and 1086 cm^{-1} to the -C-C- stretching vibrations. The band located at 1376 cm^{-1} is connected with the deformation -OH band occurring in alcohols. In addition, in all investigated samples, the bands placed between 1600 and 1680 cm^{-1} are visible. They are the fingerprints of the stretching vibration bands of the C=C functional group. Furthermore, in the IR spectra located between 1667 and 2000 cm^{-1} one can distinguish additional bands assigned to the bending vibrations involved in the CH=CH$_2$ group. The obtained FT-IR results agree well with the GC-MS analysis performed for the investigated systems. The IR spectra obtained for the liquid products characterized by high ratio of iso-/n-alkane do not show any stretching vibration bands of C-H in aliphatic hydrocarbons (e.g., Spent-Red-Mi-Ni$_{3.0}$Co$_{10}$SiBeta and Spent-Red-Mi-Ni$_{3.0}$Co$_{10}$AlBeta). Furthermore, the IR spectra of the liquid product which contains high ratio of unsaturated to saturated hydrocarbons obtained using Spent-Red-Mi-Ni$_{3.0}$Co$_{10}$SiBeta catalyst indicate high intensity of the specific bands related to the stretching vibrations in C=C functional group.
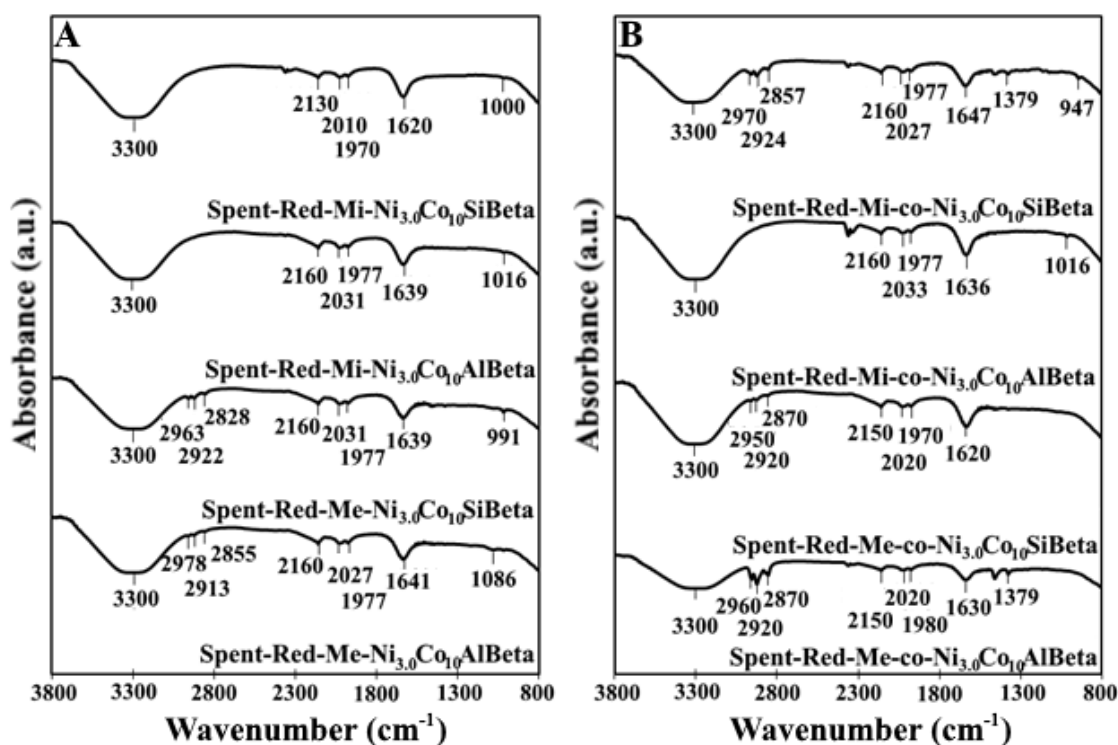
Figure 12. FT-IR spectra of obtained liquid products over (**A**) Spent-Red-Me-Ni$_{3.0}$Co$_{10}$AlBeta, Spent-Red-Mi-Ni$_{3.0}$Co$_{10}$AlBeta, Spent-Red-Me-Ni$_{3.0}$Co$_{10}$SiBeta, Spent-Red-Me-Ni$_{3.0}$Co$_{10}$SiBeta and (**B**) Spent-Red-Me-co-Ni$_{3.0}$Co$_{10}$AlBeta, Spent-Red-Mi-co-Ni$_{3.0}$Co$_{10}$AlBeta, Spent-Red-Me-co-Ni$_{3.0}$Co$_{10}$SiBeta, Spent-Red-Me-co-Ni$_{3.0}$Co$_{10}$SiBeta.

3. Materials and Methods

3.1. Materials Preparation

Ni$_{3.0}$Co$_{10}$AlBeta and Ni$_{3.0}$Co$_{10}$SiBeta zeolites were obtained by conventional wet impregnation and two-step postsynthesis method, respectively. In order to obtain these zeolites, micro- and mesoporous tetraethylammonium Beta (TEABeta) zeolites produced by RIPP (Beijing, China) divided on two fractions and prepared as described in Section 2.1.

3.2. Characterization Study

3.2.1. Chemical Analysis

The cobalt and nickel contents as well as Si/Al ratio of examined samples were determined at room temperature by X-ray Fluorescence (XRF) (SPECTRO X-LabPro apparatus, Kleve, Germany)

3.2.2. XRD

The XRD study was performed on a PANalytical X'Pert Pro diffractometer (Malvern Panalytical Ltd., Malvern, UK) using Cu Kα radiation (λ = 154.05 pm) in 2θ range of 5–90°.

3.2.3. XPS

The X-ray Photoelectron Spectroscopy (XPS) experiments were carried out with a hemispherical analyzer (SES R4000, GammadataScienta, (GammadataScienta, Uppsala, Sweden). The non-monochromatized Al Kα source (12 kV, 15 mA) was used to generate photoelectron excitations. The spectrometer was calibrated in accordance with ISO 15472:2001. The energy resolution of the system, measured as a full width at half maximum (FWHM) for Ag 3d$_{5/2}$ excitation line, was 0.9 eV

(pass energy 100 eV). During the measurements, the base pressure in the analysis chamber was ca. 2×10^{-9} mbar. The survey scans were obtained at pass energy of 200 eV (with 0.25 eV step), whereas high-resolution spectra were gathered at pass energy of 100 eV (with 25 meV step). The area of sample investigation was about 3 mm^2. The experimental curves were fitted, after subtraction of the Shirley-type background, with a combination of Gaussian and Lorentzian lines of a constant proportion (70:30) with the use of CasaXPS 2.3.19 software. The Co 2p and Ni 2p lines were deconvoluted with a relative intensity ratio of 2p$_{3/2}$ and 2p$_{1/2}$ components fixed to 2:1. The BE values were charge-corrected to the carbon C 1s excitation which was set at 285.0 eV.

3.2.4. NH$_3$-TPD

The number and strength of acidic sites of tested samples were investigated by temperature-programmed desorption of ammonia (NH$_3$-TPD) in a quartz reactor. First, ca. 0.1 g of the sample was heated at 500 °C in argon flow for 1 h. Next, the gaseous ammonium was adsorbed on the sample at 100 °C for 15 min, and then physically adsorbed NH$_3$ was removed from the CoBeta systems by argon flow for 15 min. The measurement was performed in the temperature range of 40–600 °C. In addition, to evaluate the effect of metal reduction on the sample acidity, bimetallic systems reduced at 400 °C for 1 h were examined by the adsorption of ammonia gas. The amount of adsorbed ammonia was detected using a thermal conductivity detector (Altamira Instruments, Pittsburgh, PA, USA).

3.2.5. TPR-H$_2$

The TPR-H$_2$ profiles of tested systems (0.1 g) were performed in an automatic TPR system. The flow of reducing mixture (5% H$_2$–95% Ar) was 40 mL min^{-1} (Air Products Ltd., Warsaw, Poland). The quantitative consumption of the H$_2$ was overseen by a thermal conductivity detector (TCD) (Altamira Instruments, Pittsburgh, PA, USA). The measurement was carried out in the temperature range of 25–900 °C (with 10 °C min^{-1} ramp rate).

3.2.6. TEM-EDS

A Transmission Electron Microscopy (TEM) study was realised on a JEOL JEM 2100 FEG microscope (Tokyo, Japan) operating at 200 kV with a spatial punctual resolution of 1.8 Å equipped with X-ray Energy Dispersive Spectroscopy (EDS) for chemical analysis. The samples were prepared by depositing a drop of the ultrasonically dispersed powder in ethanol on the carbon film of Cu grid.

3.3. Catalytic Activity

The Scheme 2 of the experimental set-up used for FT synthesis is presented below.

Before Fischer–Tropsch synthesis, in situ reduction of all catalysts was conducted in H$_2$ flow (40 mL min^{-1}) at an atmospheric pressure at 500 °C for 1 h, then the temperature was decreased to 260 °C in flow of H$_2$. After that, the reaction conditions (T = 260 °C, p = 30 atm and CO:H$_2$ ratio of 1:2 with H$_2$ flow of 40 mL min^{-1} and CO$_2$ flow of 20 mL min^{-1}) were set and catalysts were stabilized by night in these conditions. The Fischer–Tropsch synthesis over Ni$_{3.0}$Co$_{10}$Beta and co-Ni$_{3.0}$Co$_{10}$Beta zeolite systems (0.5 g) was carried out at a stainless steel fix-bed flow reactor at 30 atm in 260 °C for 24 h. The flow reactor with a length of 50 cm and an internal diameter of 7 mm was located in a 35 cm length furnace. The catalyst bed bulk height was 5.8 cm and it was situated in the middle of the reactor.

The molar ratio of the reaction mixture (CO/H$_2$) was 1:2. The total reactants flow during the reaction was 60 mL min^{-1}. Obtained gaseous products were analyzed by a GC gas chromatograph (Shimadzu GC-14, Duisburg, Germany) supplied with two columns (measuring—Carbosphere 7A an comparative one—molecular sieves 7B) and two detectors—thermal conductivity (TCD) and flame ionization (FID). The chromatograph was operated with temperature of column −45 °C, detector −120 °C and injector −120 °C. Liquid products of Fischer–Tropsch synthesis were examined by the GC–MS coupled method (6890 N Network GC System with a ZB-1MS capillary column—a length of 30 m, an internal diameter of 0.25 mm linked with a 5973 Network Mass Selective Detector mass spectrometer with a 7683 Series

Injector autosampler (AGILENT, Midland, ON, Canada). The chromatographic analysis was carried out in the temperature range of 70–250 °C (8 °C min^{-1}). The initial and final temperatures of the analysis were held for 3 and 30 min, respectively. Based on the Anderson–Schultz–Floury (ASF) distribution of liquid products, the value of chain growth probability (α) was calculated. The ASF equation, in the case of non-dependence of α from the hydrocarbon chain length, can be represented as follows:

$$\log(W_n/n) = n\log\alpha + const.$$

where W_n is the mass fraction of the species with carbon number n.

The value of α was obtained from the slope of log (W_n/n) against n plot.

The activity and selectivity to C_1-C_4 (SCH_4), CO_2 (SCO_2), and liquid products (SLP) were calculated by using the formulas provided below:

$$K_{co} = ((S_{coin} - S_{COari})/S_{COin}) \times 100\%$$

$$S_{CH4} = ((X_{CH4} \times 100\%)/X_{CH4out})/F$$

$$X_{CH4out} = (X_{CH4s} \times K_{CO})/100\%$$

$$S_{CO2out} = ((X_{CO2i} \times 100\%)/X_{CO2out})/F$$

$$X_{CO2out} = (X_{CO2s} \times K_{CO})/100\%$$

$$F = S_{Ar\,i}/S_{Ar\,s}$$

$$S_{LP} = 100 - (S_{CH4} + S_{CO2})$$

where: K_{CO}—conversion of CO, S_{COin}—CO peak area before reaction, S_{COari}—CO peak area after reaction, S_{CH4}—selectivity to CH_4, S_{CO2}—selectivity to CO_2, X_{CH4i}—peak area of obtained CH_4, X_{CO2i}—peak area of obtained CO_2, X_{CH4out}—theoretical CH_4 peak area, when all CO is converted to CH_4, X_{CO2out}—theoretical CO_2 peak area, when all CO is converted to CO_2, X_{CH4s}—standard CH_4 area, when only CH_4 is tested, X_{CO2s}—standard CO_2 area, when only CO_2 is tested, F—contraction coefficient, S_{Ari}—Ar peak area during reaction, S_{Ars}—Ar peak area before reaction, S_{LP}—selectivity to liquid products.
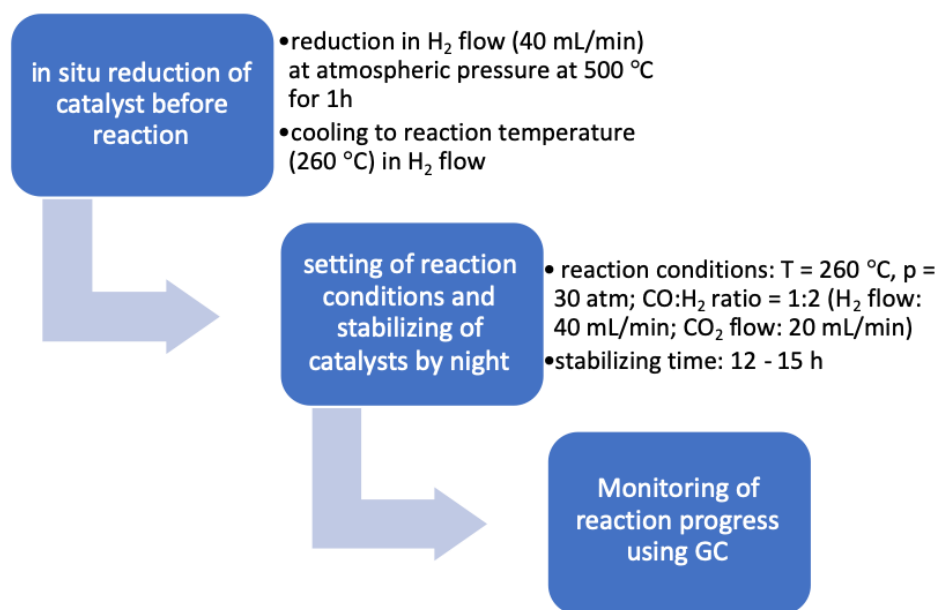
Scheme 2. The scheme of the experimental set-up used for FT synthesis.

The analysis of liquid products formed during the hydrogenation of CO was carried out on the IRTracer-100 FTIR (Shimadzu, Duisburg, Germany) spectrometer equipped with a liquid nitrogen cooled MCT detector. To achieve a good signal to noise ratio, 128 scans with 4 cm^{-1} resolution were collected. The "Specac" reliable ATR accessory was applied in all the measurements.

4. Conclusions

The impact of Ni addition on the efficiency of cobalt based zeolite catalysts prepared with two types of Beta zeolite in FTS was determined in the present paper. The work shows that the presence of the Ni promoter led to a decrease in the temperature of the cobalt oxide reduction and an increase of the CO conversion.

Neither the dealumination of Beta zeolite nor the incorporation of Co and Ni affected its structure.

Among all tested catalysts, the highest activity in FTS were found for the Red-Mi-Ni$_{3.0}$Co$_{10}$SiBeta and Red-Mi-co-Ni$_{3.0}$Co$_{10}$SiBeta, for which a very high CO conversion near 100% and selectivity to liquid products of about 75% were achieved.

The nickel addition stabilizes a catalytic system during the whole time of synthesis (24 h).

In case of dealuminated samples, the presence of Ni promoter led to a decrease in the selectivity to liquid products.

References

1. Wu, L.; Li, Z.; Han, D.; Wu, J.; Zhang, D. A preliminary evaluation of ZSM-5/SBA-15 composite supported Co catalysts for Fischer–Tropsch synthesis. *Fuel Process. Technol.* **2015**, *134*, 449–455. [CrossRef]
2. Wang, S.; Yin, Q.; Guo, J.; Ru, B.; Zhu, L. Improved Fischer–Tropsch synthesis for gasoline over Ru, Ni promoted Co/HZSM-5 catalysts. *Fuel* **2013**, *108*, 597–603. [CrossRef]
3. Moodley, D.J.; van de Loosdrecht, J.; Saib, A.M.; Overett, M.J.; Datye, A.K.; Niemantsverdriet, J.W. Carbon deposition as a deactivation mechanism of cobalt-based Fischer–Tropsch synthesis catalysts under realistic conditions. *Appl. Catal. A Gen.* **2009**, *354*, 102–110. [CrossRef]
4. Sartipi, S.; Parashar, K.; Valero-Romero, M.J.; Santos, V.P.; van der Linden, B.; Makkee, M.; Kapteijn, F.; Gascon, J. Hierarchical H-ZSM-5-supported cobalt for the direct synthesis of gasoline-range hydrocarbons from syngas: Advantages, limitations, and mechanistic insight. *J. Catal.* **2013**, *305*, 179–190. [CrossRef]
5. Concepción, P.; López, C.; Martínez, A.; Puntes, V.F. Characterization andatalytic properties of cobalt supported on delaminated ITQ-6 and ITQ-2 zeolites for the Fischer-Tropsch synthesis reaction. *J. Catal.* **2004**, *228*, 321–332. [CrossRef]
6. Jung, J.-S.; Kim, S.W.; Moon, D.J. Fischer–Tropsch Synthesis over cobalt based catalyst supported on different mesoporous silica. *Catal. Today* **2012**, *185*, 168–174. [CrossRef]
7. Najafabadi, A.T.; Khodadadi, A.A.; Parnian, M.J.; Mortazavi, Y. Atomic layer deposited Co/γ-Al$_2$O$_3$ catalyst with enhanced cobalt dispersion and Fischer–Tropsch synthesis activity and selectivity. *Appl. Catal A Gen.* **2016**, *511*, 31–46. [CrossRef]
8. Hajjar, R.; Millot, Y.; Man, P.P.; Che, M.; Dzwigaj, S. Two Kinds of Framework Al Sites Studied in BEA Zeolite by X-ray Diffraction, Fourier Transform Infrared Spectroscopy, NMR Techniques, and V Probe. *J. Phys. Chem. C* **2008**, *112*, 20167–20175. [CrossRef]
9. Baran, R.; Millot, Y.; Onfroy, T.; Krafft, J.M.; Dzwigaj, S. Influence of the nitric acid treatment on Al removal, framework composition and acidity of BEA zeolite investigated by XRD, FTIR and NMR. *Microporous Mesoporous Mater.* **2012**, *163*, 122–130. [CrossRef]
10. Pour, A.N.; Zamani, Y.; Tavasoli, A.; Shahri, S.M.K.; Taheri, S.A. Study on products distribution of iron and iron–zeolite catalysts in Fischer–Tropsch synthesis. *Fuel* **2008**, *87*, 2004–2012. [CrossRef]

11. Martinez, A.; Lopez, C. The influence of ZSM-5 zeolite composition and crystal size on the in situ conversion of Fischer–Tropsch products over hybrid catalysts. *Appl. Catal. A Gen.* **2005**, *294*, 251–259. [CrossRef]

12. Tang, Q.; Wang, Y.; Zhang, Q.; Wan, H. Preparation of metallic cobalt inside NaY zeolite with high catalytic activity in Fischer–Tropsch synthesis. *Catal. Commun.* **2003**, *4*, 253–258. [CrossRef]

13. Liu, Z.W.; Li, X.; Asami, K.; Fujimoto, K. Iso-paraffins synthesis from modified Fischer–Tropsch reaction—Insights into Pd/beta and Pt/beta catalysts. *Catal. Today* **2005**, *104*, 41–47. [CrossRef]

14. Chalupka, K.A.; Casale, S.; Zurawicz, E.; Rynkowski, J.; Dzwigaj, S. The remarkable effect of the preparation procedure on the catalytic activity of CoBEA zeolites in the Fischer–Tropsch synthesis. *Microporous Mesoporous Mater.* **2015**, *211*, 9–18. [CrossRef]

15. Chalupka, K.A.; Maniukiewicz, W.; Mierczynski, P.; Maniecki, T.; Rynkowski, J.; Dzwigaj, S. The catalytic activity of Fe-containing SiBEA zeolites in Fischer–Tropsch synthesis. *Catal. Today* **2015**, *257*, 117–121. [CrossRef]

16. Park, J.-Y.; Lee, Y.-J.; Karandikar, P.R.; Jun, K.-W.; Ha, K.-S.; Park, H.-G. Fischer–Tropsch catalysts deposited with size-controlled Co_3O_4 nanocrystals: Effect of Co particle size on catalytic activity and stability. *Appl. Catal. A Gen.* **2012**, *411*, 15–23. [CrossRef]

17. Xiong, H.; Zhang, Y.; Liew, K.; Li, J. Catalytic performance of zirconium-modified Co/Al_2O_3 for Fischer–Tropsch synthesis. *J. Mol. Catal. A Chem.* **2005**, *231*, 145–151. [CrossRef]

18. Ali, S.; Chen, B.; Goodwin, J.G., Jr. Zr Promotion of Co/SiO_2 for Fischer-Tropsch Synthesis. *J. Catal.* **1995**, *157*, 35–41. [CrossRef]

19. Xu, D.; Li, W.; Duan, H.; Ge, Q.; Xu, H. Reaction performance and characterization of Co/Al_2O_3 Fischer–Tropsch catalysts promoted with Pt, Pd and Ru. *Catal. Lett.* **2005**, *102*, 229–235. [CrossRef]

20. Vada, S.; Hoff, A.; Ådnanes, E.; Schanke, D.; Holmen, A. Fischer-Tropsch synthesis on supported cobalt catalysts promoted by platinum and rhenium. *Top. Catal.* **1995**, *2*, 155–162. [CrossRef]

21. Das, T.K.; Jacobs, G.; Patterson, P.M.; Conner, W.A.; Li, J.; Davis, B.H. Fischer–Tropsch synthesis: Characterization and catalytic properties of rhenium promoted cobalt alumina catalysts. *Fuel* **2003**, *82*, 805–815. [CrossRef]

22. Jacobs, G.; Chaney, J.A.; Patterson, P.M.; Das, T.K.; Davis, B.H. Fischer–Tropsch synthesis: Study of the promotion of Re on the reduction property of Co/Al_2O_3 catalysts by in situ EXAFS/XANES of Co K and Re LIII edges and XPS. *Appl. Catal. A Gen.* **2004**, *264*, 203–212. [CrossRef]

23. Xiong, H.; Zhang, Y.; Liew, K.; Li, J. Ruthenium promotion of Co/SBA-15 catalysts with high cobalt loading for Fischer–Tropsch synthesis. *Fuel Process. Technol.* **2009**, *90*, 237–246. [CrossRef]

24. Rytter, E.; Skagseth, T.H.; Eri, S.; Sjåstad, A.O. Cobalt Fischer−Tropsch Catalysts Using Nickel Promoter as a Rhenium Substitute to Suppress Deactivation. *Ing. Eng. Chem. Res.* **2010**, *49*, 4140–4148. [CrossRef]

25. Sadek, R.; Chalupka, K.A.; Mierczynski, P.; Rynkowski, J.; Millot, Y.; Valentin, L.; Casale, S.; Dzwigaj, S. Fischer-Tropsch reaction on Co-containing microporous and mesoporous Beta zeolite catalysts: The effect of porous size and acidity. *Catal. Today* **2019**. [CrossRef]

26. Dzwigaj, S.; Che, M. Incorporation of Co(II) in Dealuminated BEA Zeolite at Lattice Tetrahedral Sites Evidenced by XRD, FTIR, Diffuse Reflectance UV−Vis, EPR, and TPR. *J. Phys. Chem. B* **2006**, *110*, 12490–12493. [CrossRef]

27. Mintova, S.; Valtchev, V.; Onfroy, T.; Marichal, C.; Knözinger, H.; Bein, T. Variation of the Si/Al ratio in nanosized zeolite Beta crystals. *Microporous Mesoporous Mater.* **2006**, *90*, 237–245. [CrossRef]

28. Chalupka, K.A.; Jozwiak, W.K.; Rynkowski, J.; Maniukiewicz, W.; Casale, S.; Dzwigaj, S. Partial oxidation of methane on NixAlBEA and NixSiBEA zeolite catalysts: Remarkable effect of preparation procedure and Ni content. *Appl. Catal. B Environ.* **2014**, *146*, 227–236. [CrossRef]

29. Dzwigaj, S.; Janas, J.; Machej, T.; Che, M. Selective catalytic reduction of NO by alcohols on Co- and Fe-Siβ catalysts. *Catal. Today* **2007**, *119*, 133–136. [CrossRef]

30. Fazlollahi, F.; Sarkari, M.; Zare, A.; Mirzaei, A.A.; Atashi, H. Development of a kinetic model for Fischer–Tropsch synthesis over $Co/Ni/Al_2O_3$ catalyst. *J. Ind. Eng. Chem.* **2012**, *18*, 1223–1232. [CrossRef]

31. Erdogan, B.; Arbag, H.; Yasyerli, N. SBA-15 supported mesoporous Ni and Co catalysts with high coke resistance for dry reforming of methane. *Int. J. Hydrogen Energy* **2018**, *43*, 1396–1405. [CrossRef]

32. Mosayebi, A.; Abedini, R. Detailed kinetic study of Fischer—Tropsch synthesis for gasoline production over Co-Ni/HZSM-5 nano-structure catalyst. *Int. J. Hydrogen Energy* **2017**, *42*, 27013–27023. [CrossRef]

33. Rodriguez-Gomez, A.; Caballero, A. Bimetallic Ni-Co/SBA-15 catalysts for reforming of ethanol: How cobalt modifies the nickel metal phase and product distribution. *Mol. Catal.* **2018**, *449*, 122–130. [CrossRef]

34. Arbag, H.; Yasyerli, S.; Yasyerli, N.; Dogu, G.; Dogu, T. Enhancement of catalytic performance of Ni based mesoporous alumina by Co incorporation in conversion of biogas to synthesis gas. *Appl. Catal. B Environ.* **2016**, *198*, 254–265. [CrossRef]

35. Boroń, P.; Chmielarz, L.; Gurgul, J.; Łątka, K.; Shishido, T.; Krafft, J.-M.; Dzwigaj, S. BEA zeolite modified with iron as effective catalyst for N2O decomposition and selective reduction of NO with ammonia. *Appl. Catal. B Environ.* **2013**, *138*, 434–445. [CrossRef]

36. Boroń, P.; Chmielarz, L.; Gurgul, J.; Łątka, K.; Gil, B.; Krafft, J.-M.; Dzwigaj, S. The influence of the preparation procedures on the catalytic activity of Fe-BEA zeolites in SCR of NO with ammonia and N_2O decomposition. *Catal. Today* **2014**, *235*, 210–225. [CrossRef]

37. Kocemba, I.; Rynkowski, J.; Gurgul, J.; Socha, R.P.; Łątka, K.; Krafft, J.-M.; Dzwigaj, S. Nature of the active sites in CO oxidation on FeSiBEA zeolites. *Appl. Catal. A Gen.* **2016**, *519*, 16–26. [CrossRef]

38. Kumar, M.S.; Schwidder, M.; Grünert, W.; Bentrup, U.; Brückner, A. Selective reduction of NO with Fe-ZSM-5 catalysts of low Fe content: Part II. Assessing the function of different Fe sites by spectroscopic in situ studies. *J. Catal.* **2006**, *239*, 173–186.

39. Arishtirova, K.; Kovacheva, P.; Predoeva, A. Activity and basicity of BaO modified zeolite and zeolite-type catalysts. *Appl. Catal. A Gen.* **2003**, *243*, 191–196. [CrossRef]

40. Kovacheva, P.; Arishtirova, K.; Predoeva, A. Basic zeolite and zeolite-type catalysts for the oxidative methylation of toluene with methane. *React. Kinet. Catal. Lett.* **2003**, *79*, 149–155. [CrossRef]

41. Oleksenko, L.P. Characteristics of Active Site Formation in Co-Containing Catalysts for CO Oxidation on Chemically Different Supports. *Theor. Exp. Chem.* **2004**, *40*, 331–336. [CrossRef]

42. Grünert, W.; Schlögl, R. Photoelectron Spectroscopy of Zeolites. *Mol. Sieves* **2004**, *4*, 467–515.

43. Janas, J.; Gurgul, J.; Socha, R.P.; Dzwigaj, S. Effect of Cu content on the catalytic activity of CuSiBEA zeolite in the SCR of NO by ethanol: Nature of the copper species. *Appl. Catal. B Environ.* **2009**, *91*, 217–224. [CrossRef]

44. Gurgul, J.; Łątka, K.; Hnat, I.; Rynkowski, J.; Dzwigaj, S. Identification of iron species in FeSiBEA by DR UV-vis, XPS and Mössbauer spectroscopy: Influence of Fe content. *Microporous Mesoporous Mater.* **2013**, *168*, 1–6. [CrossRef]

45. Boroń, P.; Chmielarz, L.; Gurgul, J.; Łątka, K.; Gil, B.; Marszałek, B.; Dzwigaj, S. Influence of iron state and acidity of zeolites on the catalytic activity of FeHBEA, FeHZSM-5 and FeHMOR in SCR of NO with NH3 and N2O decomposition. *Microporous Mesoporous Mater.* **2015**, *203*, 73–85. [CrossRef]

46. Kim, J.-G.; Pugmire, D.L.; Battaglia, D.; Langell, M.A. Analysis of the $NiCo_2O_4$ spinel surface with Auger and X-ray photoelectron spectroscopy. *Appl. Surf. Sci.* **2000**, *165*, 70–84. [CrossRef]

47. Rodríguez, J.L.; Valenzuela, M.A.; Poznyak, T.; Lartundo, L.; Chairez, I. Reactivity of NiO for 2,4-D degradation with ozone: XPS studies. *J. Hazard. Mater.* **2013**, *262*, 472–481. [CrossRef]

48. NIST X-ray Photoelectron Spectroscopy Database. Available online: http://srdata.nist.gov/xps/ (accessed on 15 September 2012).

49. Langell, M.A.; Anderson, M.D.; Carson, G.A.; Peng, L.; Smith, S. Valence-band electronic structure of Co_3O_4 epitaxy on CoO (100). *Phys. Rev. B* **1999**, *59*, 4791–4798. [CrossRef]

50. Tan, B.J.; Klabunde, K.J.; Sherwood, P.M.A. XPS studies of solvated metal atom dispersed (SMAD) catalysts. Evidence for layered cobalt-manganese particles on alumina and silica. *J. Am. Chem. Soc.* **1991**, *113*, 855–861. [CrossRef]

51. Zhou, Z.; Zhang, Y.; Wang, Z.; Wei, W.; Tang, W.; Shi, J.; Xiong, R. Electronic structure studies of the spinel $CoFe_2O_4$ by X-ray photoelectron spectroscopy. *Appl. Surf. Sci.* **2008**, *254*, 6972–6975. [CrossRef]

52. Ivanova, T.; Naumkin, A.; Sidorov, A.; Eremenko, I.; Kiskin, M. X-ray photoelectron spectra and electron structure of polynuclear cobalt complexes. *J. Electron. Spectrosc. Relat. Phenom.* **2007**, *156*, 200–203. [CrossRef]

53. Chen, H.-H.; Shen, S.-C.; Chen, X.; Kawi, S. Selective catalytic reduction of NO over Co/beta-zeolite: Effects of synthesis condition of beta-zeolites, Co precursor, Co loading method and reductant. *Appl. Catal. B Environ.* **2004**, *50*, 37–47. [CrossRef]

54. Janas, J.; Machej, T.; Gurgul, J.; Socha, R.P.; Che, M.; Dzwigaj, S. Effect of Co content on the catalytic activity of CoSiBEA zeolite in the selective catalytic reduction of NO with ethanol: Nature of the cobalt species. *Appl. Catal. B Environ.* **2007**, *75*, 239–248. [CrossRef]

55. Zsoldos, Z.; Vass, G.; Lu, G.; Guczi, L. XPS study on the effects of treatments on Pt^{2+} and Co^{2+} exchanged into NaY zeolite. *Appl. Surf. Sci.* **1994**, *78*, 467–475. [CrossRef]

56. Da Cruz, R.S.; Mascarenhas, A.J.S.; Andrade, H.M.C. Co-ZSM-5 catalysts for N_2O decomposition. *Appl. Catal. B Environ.* **1998**, *18*, 223–231. [CrossRef]

57. Janas, J.; Gurgul, J.; Socha, R.P.; Kowalska, J.; Nowinska, K.; Shishido, T.; Che, M.; Dzwigaj, S. Influence of the Content and Environment of Chromium in CrSiBEA Zeolites on the Oxidative Dehydrogenation of Propane. *J. Phys. Chem. C* **2009**, *113*, 13273–13281. [CrossRef]

58. Dzwigaj, S.; Janas, J.; Mizera, J.; Gurgul, J.; Socha, R.P.; Che, M. Incorporation of Copper in SiBEA Zeolite as Isolated Lattice Mononuclear Cu(II) Species and its Role in Selective Catalytic Reduction of NO by Ethanol. *Catal. Lett.* **2008**, *126*, 36–42. [CrossRef]

59. Boroń, P.; Chmielarz, L.; Casal, S.; Calers, C.; Krafft, J.-M.; Dzwigaj, S. Effect of Co content on the catalytic activity of CoSiBEA zeolites in N_2O decomposition and SCR of NO with ammonia. *Catal. Today* **2015**, *258*, 507–517. [CrossRef]

60. Stanton, A.R.; Iisa, K.; Yung, M.M.; Magrini, K.A. Catalytic fast pyrolysis with metal-modified ZSM-5 catalysts in inert and hydrogen atmospheres. *J. Anal. Appl. Pyrol.* **2018**, *135*, 199–208. [CrossRef]

61. Lim, T.H.; Cho, S.J.; Yang, H.S.; Engelhard, M.H.; Kim, D.H. Effect of Co/Ni ratios in cobalt nickel mixed oxide catalysts on methane combustion. *Appl. Catal. A Gen.* **2015**, *505*, 62–69. [CrossRef]

62. Nieto-Márquez, A.; Lazo, J.C.; Romero, A.; Valverde, J.L. Growth of nitrogen-doped filamentous and spherical carbon over unsupported and Y zeolite supported nickel and cobalt catalysts. *Chem. Eng. J.* **2008**, *144*, 518–530. [CrossRef]

63. Ochoa-Hernández, C.; Yang, Y.; Pizarro, P.; de la Peña O'Shea, V.A.; Coronado, J.M.; Serrano, D.P. Hydrocarbons production through hydrotreating of methyl esters over Ni and Co supported on SBA-15 and Al-SBA-15. *Catal. Today* **2013**, *210*, 81–88. [CrossRef]

64. Sadek, R.; Chalupka, K.A.; Mierczynski, P.; Rynkowski, J.; Gurgul, J.; Dzwigaj, S. Cobalt Based Catalysts Supported on Two Kinds of Beta Zeolite for Application in Fischer-Tropsch Synthesis. *Catalysts* **2019**, *9*, 497. [CrossRef]

65. Shimura, K.; Miyazawa, T.; Hanaoka, T.; Hirata, S. Fischer–Tropsch synthesis over alumina supported bimetallic Co–Ni catalyst: Effect of impregnation sequence and solution. *J. Mol. Catal. A Chem.* **2015**, *407*, 15–24. [CrossRef]

66. Cheng, J.; Hu, P.; Ellis, P.; French, S.; Kelly, G.; Lok, C.M. A DFT study of the chain growth probability in Fischer–Tropsch synthesis. *J. Catal.* **2008**, *257*, 221–228. [CrossRef]

67. Socrats, G. Infrared Characteristic Group Frequencies. In *Tables and Charts*, 2nd ed.; Wiley: Chichester, UK, 1994; pp. 1–249.